Title

Ligand Control of Structural Diversity in Luminescent Hybrid Copper(I) Iodides

Journal

Chemistry of Materials, 34(7)

ISSN

0897-4756 1520-5002

Authors

Wang, Shuxin
Morgan, Emily E
Panuganti, Shobhana
et al.

Publication Date

2022-03-14

DOI

10.1021/acs.chemmater.1c04408

Peer reviewed

Ligand Control of Structural Diversity in Luminescent Hybrid Copper (I) Iodides

Shuxin Wang,[1,2] Emily E. Morgan,[1] Shobhana Panuganti,[3] Lingling Mao,[4] Pratap Vishnoi,[5] Guang Wu,[6] Quanlin Liu,[2] Mercouri G. Kanatzidis,[3,7] Richard D. Schaller,[3,8] Ram Seshadri[1,6]*

[1]Materials Department and Materials Research Laboratory
University of California, Santa Barbara, California 93106, United States

[2]The Beijing Municipal Key Laboratory of New Energy Materials and Technologies,
School of Materials Sciences and Engineering
University of Science and Technology Beijing, Beijing 100083, China

[3]Department of Chemistry
Northwestern University, Evanston, Illinois 60208, United States

[4]Department of Chemistry' Southern University of Science and Technology, Guangdong Shenzhen, 518055 China

5 New Chemistry Unit & International Centre for Materials Science, Jawaharlal Nehru Centre for Advanced Scientific Research, New Chemistry Unit, Jakkur, Bangalore, 560064 India

[6]Department of Chemistry and Biochemistry
University of California Santa Barbara, California 93106, United States

[7]Material Science Division
Argonne National Laboratory, Lemont, Illinois 60439, United States

[8]Center for Nanoscale Materials
Argonne National Laboratory, Lemont, Illinois 60439, United States

ABSTRACT: Copper (I) iodide hybrids are of interest for next-generation lighting technologies because of their efficient luminescence in the absence of rare-earths. Here, we report ten structurally diverse hybrid copper (I) iodides that emit in the green-red region with quantum yields reaching 67 %. The compounds display a diversity of structures including ones with 1D Cu–1 chains, Cu_2I_2 rhomboid dimers, and structures with two different arrangements of Cu_4I_4 tetramers. The compounds with Cu_2I_2 rhomboid dimers or Cu_4I_4 cubane tetramer have higher photoluminescence quantum yield than those with Cu–I 1D chain and octahedral Cu_4I_4 tetramer, owing to the optimal degree of condensation of the inorganic motifs that suppresses non-radiative processes. Electronic structure calculations on these compounds point out the critical influence of the inorganic motif and organic ligand on the nature of the band gaps and thus the excitation characteristics. Temperature dependent photoluminescence spectra are presented to better understand the nature of luminescence in compounds with different inorganic motifs. The emerging understanding of composition-structure-property correlations in this family provide inspiration for the rational design of hybrid phosphors for general lighting applications.

INTRODUCTION

Hybrid materials have established themselves as one of the leading functional materials classes because of their rich structural diversity, fascinating physical properties, and wide potential applications.[1-6] The integration of the inorganic modules and organic templates enables the combination of the superior optical, electrical, and magnetic properties of the inorganic compounds with the excellent structural flexibility, solution-processability, and tunability of organic templates, providing greatly enhanced structural, chemical and physical properties.[7-12] The diverse nature of the organic templates and inorganic modules leads

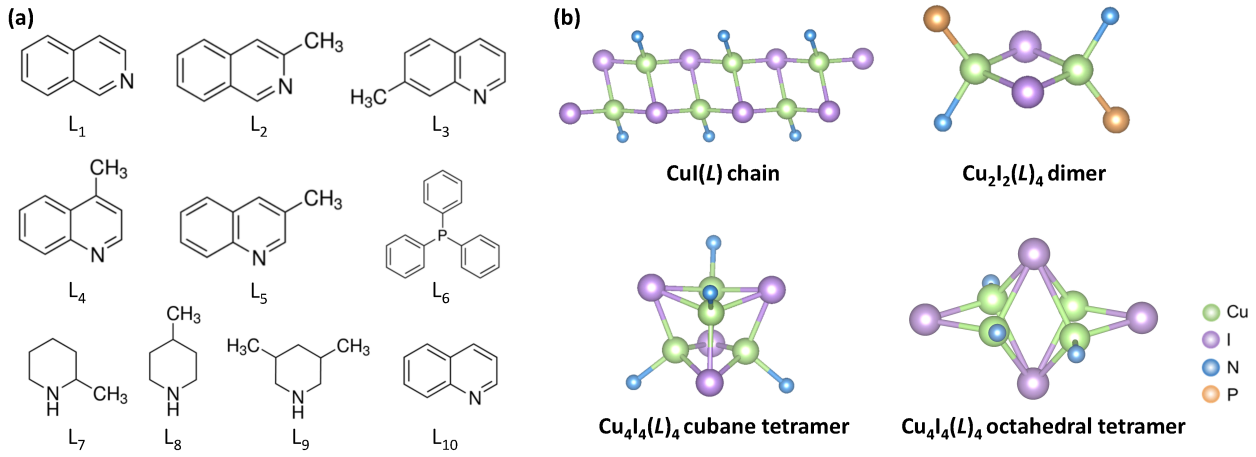

Figure 1. Illustrations of (a) ligands L_1-L_{10} used in the series of hybrid copper (I) iodides, (b) inorganic motifs of CuI 1D chain, Cu_2I_2 rhomboid dimer, Cu_4I_4 cubane tetramer, and Cu_4I_4 octahedral tetramer structures.

hybrid materials to be highly tunable, attracting tremendous research efforts to extensively explore their structural diversity and optimize their functional performance.[13-18]

The luminescence of inorganic-organic hybrid materials has attracted much attention and been extensively explored due to their rare-earth free, energy efficient, and solution processable advantages.[19-23] Copper(I) iodide hybrids are of particular interest, and regarded as promising for next generation lighting technologies because of their unique properties including structural diversity, optical tunability, and superior luminescence performance.[24-28] Aside from the diversity of the organic components, the charge-neutral inorganic motif Cu_mI_m takes various forms ranging from zero-dimensional (0D) discrete clusters[29] to one-dimensional (1D) extended chains,[30] two-dimensional (2D) layers,[31] and three-dimensional (3D) networks[32] with the most common inorganic modules being CuI monomer,[33-35] CuI 1D chains,[36-38] Cu_2I_2 rhomboid dimer,[39-41] and Cu_4I_4 cubane tetramers.[42-44] The $Cu_xI_xL_y$ complexes (L = N-, P-, S-, Sb- or Se- doner ligands) with Cu_3I_3 trimer,[45, 46] octahedral Cu_4I_4 tetramer,[47-49] Cu_4I_4 staircase tetramer,[50] and Cu_6I_6 cubane hexamer[51, 52] as inorganic modules are also reported. They are less-studied presumably due to the difficulty in synthesis. According to the theoretical calculations by Liu et al., it is proposed that the octahedral Cu_4I_4 cores are energetically unfavorable relative to the Cu_4I_4 cubane motif.[53] In the limited reports, the octahedral Cu_4I_4 complexes are formed based on bidentate ligands including P^N-, P^P-, P^C-, and N^N- donors.[45, 48, 49, 53-62] The various inorganic modules in conjunction with the diverse organic ligands via coordinate bonds give rise to rich hybrid copper (I) iodide structures of various dimensionalities (0D-3D), which provide a solid foundation for their tunable luminescence with emission covering the entire visible range and NIR edge.[24, 38, 40]

With the aim of further exploring the structural diversity and luminescence properties of copper (I) iodide hybrids, we report here ten new compounds, focusing on their composition-structure-property correlations. These new structures present a library that includes CuI 1D chain structures, Cu_2I_2 rhomboid dimer structures, Cu_4I_4 cubane tetramer structures, and octahedral Cu_4I_4 tetramer structures. All the compounds reported here are intensely luminescent with different excitation and emission characteristics. DFT calculations reveal the electronic structure of these compounds, pointing out the critical role of inorganic motif and organic ligand on band gap structure and thus their excitation characteristics. The luminescence mechanism of the compounds with different inorganic motifs was systematically investigated via temperature dependent photoluminescence (PL) measurements in which we observed red shifts in some spectral features while others exhibited blue shifts, suggesting different luminescence mechanisms as function of the various structure types. Notably, the compounds with Cu_2I_2 rhomboid dimer and Cu_4I_4 cubane tetramer have relatively higher quantum yield (QY) up to 67% than the rest of the examined compounds (<30%). This work points to the structural diversity of copper iodide hybrids and gives more insights into composition-structure-property correlations, providing inspirations for rational design of functional hybrid phosphors for general lighting applications.

RESULTS AND DISCUSSIONS

Crystal structures. A series of organic ligands (L_1-L_{10}, **Figure 1a**) were employed to form the hybrid copper iodides with the following formulas: CuI(isoquinoline) (**1**), CuI(3-methylisoquinoline) (**2**), CuI(7-methylquinoline) (**3**), CuI(3-methylquinoline) (**4**), CuI(4-methylquinoline) (**5**), Cu_2I_2(triphenylphosphine)$_2$(7-methylquinoline)$_2$ (**6**),

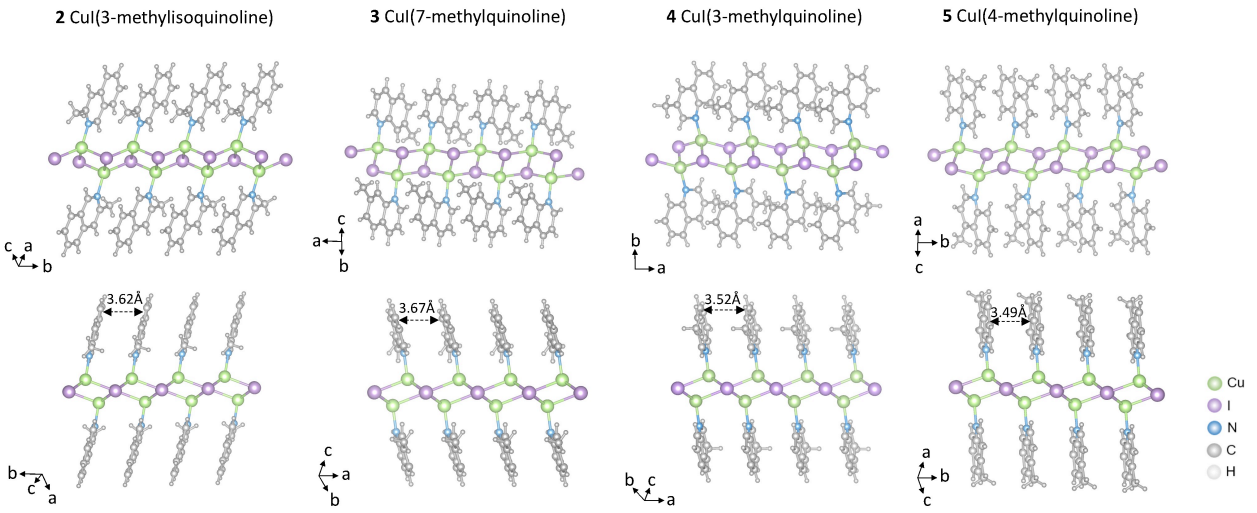

Figure 2. Crystal structures of CuI 1D chain structures **2-5** depicting one of 1D chains (top), and same structures emphasizing π···π stacking interactions (bottom).

Cu_4I_4(2-methylpiperidine)$_4$ (**7**), Cu_4I_4(4-methylpiperidine)$_4$ (**8**), Cu_4I_4(3,5-dimethylpiperidine)$_4$ (**9**), Cu_4I_4(quinoline)$_4$ (**10**). Their crystallographic and structural refinements details are summarized in **Table S1-S24**. Using powder X-ray diffraction (PXRD), the purity of the compounds was confirmed, with the diffraction patterns in excellent agreement with the calculated ones (**Figure S1**). These compounds are air and water stable. It has been demonstrated that the thermal stability of copper (I) iodide hybrids depends on their dimensionality, and the overall trend is 0D < 1D < 2D.[39, 63] The decomposition temperature for 0D and 1D copper (I) iodide hybrids is typically 50-150 ˚C.[38, 42] Compounds **1-10** with 0D/1D structures are expected to have similar thermal stability. The hybrid copper iodide compounds presented here cover a wide variety of structural types. Based on the inorganic motifs, these compounds can be categorized into four groups (**Figure 1b**): (i) CuI 1D chain structures (**1-5**); (ii) Cu_2I_2 rhomboid dimer structures (**6**); (iii) Cu_4I_4 cubane tetramer structures (**7-9**); (iv) Cu_4I_4 octahedral tetramer structures (**10**).

CuI 1D chain structures. The first group of compounds including five CuI 1D chain structures (**1-5**) were achieved with isoquinoline-, *N*-methylisoquinoline-, and *N*-methylquinoline-based organic ligands (L_1-L_5). Most of them crystallize in the monoclinic crystal system except for **2** in orthorhombic crystal system. All of them are built on 1D Cu-I chain motifs (**Figure 1b**), which further connect with organic ligands via Cu-N coordination bonds, as depicted in **Figure 2** and **S2**. Among them, organic ligand L_1 in **1** has disorder in two directions along CuI chains (**Figure S2**). The Cu-N distances in these compounds (2.000-2.064 Å) are similar to typical Cu-N bond lengths (~1.8-2.2 Å) in hybrid copper (I) iodide structures constructed via Cu-N coordination bonds.[64-68] The shortest Cu-Cu distances range from 2.796 Å to 2.865 Å, around or longer than

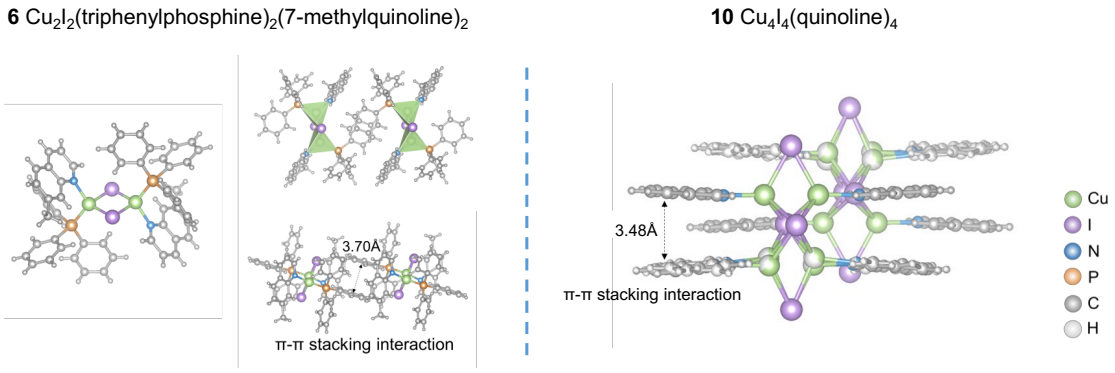

Figure 3. Crystal structures of Cu_2I_2 rhomboid dimer structure **6** (left) and Cu_4I_4 octahedral tetramer structure **10** (right).

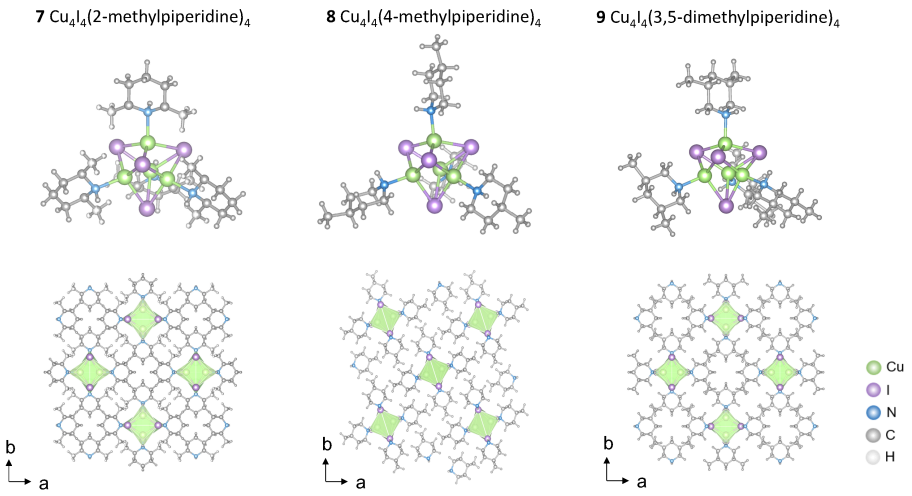

Figure 4. Crystal structures of Cu_4I_4 cubane tetramer structures **7-9** depicting one of the clusters (top); top-down view of the same structures (bottom).

twice van der Waals radius of Cu (2.80 Å), which is indicative of weak cuprophilic interaction.[69] It is worth mentioning that intermolecular forces exist between the organic ligands in these CuI 1D chain structures. There are offset π···π stacking interactions between aromatic rings with a centroid-to-centroid distance ranging from 3.49 Å to 3.67 Å, which play a critical role in stabilizing the structures, giving rise to the higher dimensional CuI 1D chain architectures.

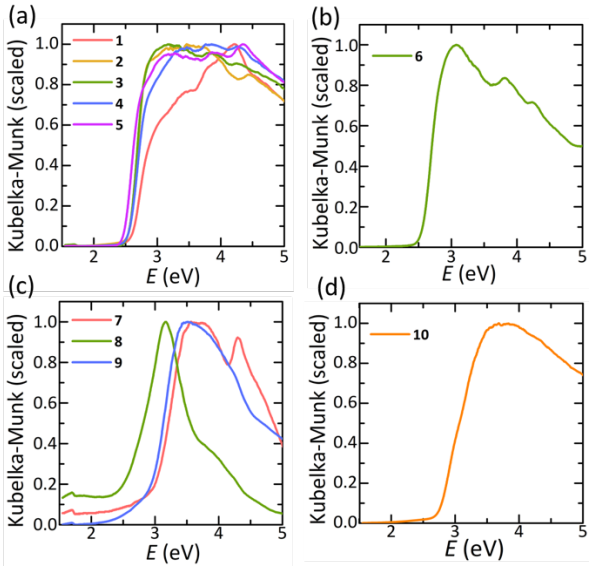

Figure 5. Optical absorption spectra of (a) CuI chain structures **1-5**, (b) Cu_2I_2 rhomboid dimer structures **6**, (c) Cu_4I_4 cubane tetramer structures **7-9**, and (d) Cu_4I_4 octahedral tetramer structures **10**. The estimated bandgaps of **1-10** range from 2.48 to 2.97 eV.

Cu_2I_2 rhomboid dimer structures. One Cu_2I_2 rhomboid dimer structure **6** was obtained through cooperation of two organic ligands, L_3 and L_6. It crystallizes in the triclinic space group $P\bar{1}$. This hybrid structure is built on Cu_2I_2 rhomboid motif (**Figure 1b**), which further connects with L_3 and L_6 via Cu-N and Cu-P coordination bonds respectively, as demonstrated in **Figure 3**. Compared with **3**, the addition of triphenylphosphine (L_6) with large size and steric hinderance breaks CuI 1D chains into low dimensional Cu_2I_2 rhomboid dimer structure. The adjacent $Cu_2I_2(L_6)_2(L_3)_2$ clusters are further interconnected by the offset π···π stacking interactions between aromatic rings with a centroid-to-centroid distance of 3.70 Å (**Figure 3**). With the incorporation of the second organic ligand L_6, the Cu-N distance (2.090 Å) in **6** is relatively longer than that in CuI chain structures (2.000-2.064 Å) due to the inductive effect. The shortest Cu-Cu distance is 3.345 Å, far longer than twice van der Waals radius of Cu (2.80 Å), which is indicative of weak cuprophilic interaction.[69]

Cu_4I_4 cubane tetramer structures. Three Cu_4I_4 cubane tetramer structures **7-9** are produced from the use of *N*-methylpiperidine and *N*, *N*'-dimethylpiperidine L_7-L_9. They all crystallize in the tetragonal crystal system. The lack of π···π stacking between aliphatic rings leads to the further separation of the architectures comprising Cu_4I_4 cubane inorganic modules (**Figure 4**). The methyl of L_7 in **7** has disorder at 2 and 6 positions on the aliphatic ring. Each copper atom in these structures is tetrahedrally coordinated to three iodine atoms and one nitrogen atom via Cu-N coordination bonds with the bond length ranging from 2.052 Å to 2.090 Å. The shortest Cu-Cu distances (2.614-2.708 Å) are shorter than twice van der Waals radius of Cu (2.80 Å), indicating strong cuprophilic interaction in Cu_4I_4 cubane tetramer structures.[69]

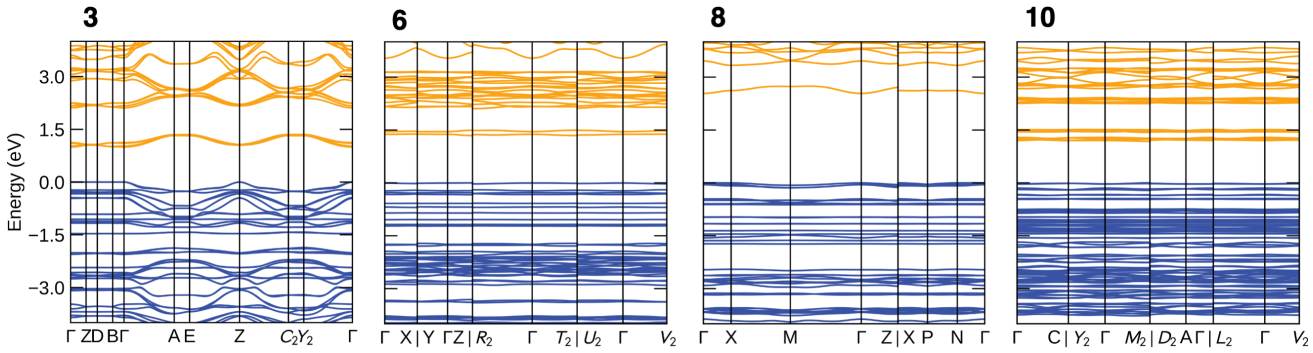

Figure 6. Band structures along high symmetry *k*-points for CuI chain structure **3**, Cu_2I_2 rhomboid dimer structure **6**, Cu_4I_4 cubane tetramer structure **8**, and Cu_4I_4 octahedral tetramer structure **10**.

Cu_4I_4 octahedral tetramer structures. An exotic type of Cu_4I_4 octahedral tetramer structure **10** comes from the use of quinoline L_{10} as organic ligand. It crystallizes in monoclinic space group C2/c. As seen in **Figure 3**, this compound possesses a rare "octahedral" geometry that differs significantly from the Cu_4I_4 cubane configurations. In the Cu_4I_4 octahedral inorganic motif, four copper atoms are arranged in a planar parallelogram, which is axially capped by two iodine atoms, forming a distorted octahedron, supplemented by two terminal iodine atoms (**Figure 1b**). The organic ligands L_{10} are connected with Cu_4I_4 octahedral inorganic modules via Cu-N coordination bonds (**Figure 3**). The Cu-N distance (1.997 Å) here is similar to the reported Cu-N bond lengths (~1.9-2.0 Å) for Cu_4I_4 octahedral tetramer structures, though studies are limited.[47, 53] Both copper and organic ligand L_{10} exhibit disorder in this structure, observed even in data collected at temperatures as low as 100 K. The shortest Cu-Cu distance is 2.158 Å, which is much shorter than twice van der Waals radius of Cu (2.80 Å), indicating extremely strong cuprophilic interaction in this compound.[69] Further analysis of the crystal stacking reveals that the adjacent organic ligands within $Cu_4I_4(L_{10})_4$ cluster are aligned by the offset π···π stacking interactions between aromatic rings with a centroid to centroid distance of 3.48 Å, which is shorter than those in CuI chain structures and Cu_2I_2 rhomboid dimer structure. The stronger offset π···π stacking interactions may be the reason for the formation of this unique Cu_4I_4 octahedral tetramer architecture instead of CuI chain configuration.

Electronic structures. Since the copper (I) iodide hybrids are potential candidate for use in future devices, it is of fundamental importance to gain insights into the electronic structures of these compounds. Based on the optical absorption spectra shown in **Figure 5**, the estimated bandgaps of **1**-**10** range from 2.48 to 2.97 eV (**Table 1**). To understand the influence of the structures and compositions on the electronic structures, DFT calculations were performed on selected compounds among the different structures. The results of the calculated band structures are summarized in **Figure 6** and **Table S25**. Compared with the dimer and tetramer structures, the band structure of **3** with CuI chain structure shows more dispersion, reflecting its more extended connectivity along the chain direction. This compound is a direct bandgap semiconductor. Given that the band structures were calculated using the PBE functional, the bandgaps shown in **Figure 6** are not quantitatively correct and tend to underestimate the experimental gaps by roughly 1.5 eV. Additionally, the band structures suggest that compounds **3**, **6**, and **10** should all have similar bandgaps, but that the gap for **8** should be significantly larger. However, the experimental absorption onset for **8** is nearly identical to that of the other compounds mentioned here. Therefore, based on the DFT and the sharpness of the peak in absorbance in the UV-vis data for **8**, we believe that the initial absorption onset in this compound is a pre-edge feature rather than representing the true bandgap of the compound. Although the intensity of this feature prevents us from determining the true bandgap of this material experimentally, trends in the band structures suggest that the true gap should be approximately 4 eV. Density of states calculations (shown in the Supporting Information) show that in all compounds, the valence band maxima are dominated by contributions from the copper 3d orbitals and iodide 5p orbitals. In the case of compound **6** there is also a small contribution from the phosphorous 3p orbitals. The conduction band minima of **3**, **6** and **10** are mostly from the π* orbitals of the aromatic ligands (carbon and nitrogen 2p orbitals), while that of **8** comprise iodine 5p orbitals due to the non-π* orbitals nature of its aliphatic ligands.

Optical properties. All these compounds exhibit photoluminescence at room temperature, as shown in **Figure 7**. The emission color can be tuned from green to red with quantum yield (QY) ranging from 1% to 67% depending on the inorganic module and organic ligand manipulation. The full width at half maximum (FWHM) of the emission bands is in the range of 78 nm to 198 nm. Compound 5 exhibits the narrowest FWHM of 78 nm. Detailed excitation energies, the corresponding emission peaks, and

FWHM are listed in **Table 1**. The room temperature lifetimes vary from 0.5 to 53.9 μs (**Table 1, Figure S3**), corresponding to their phosphorescence characteristics attributed to singlet-triplet transitions involving metal/halide-to-ligand charge transfer (^{3}M/XLCT) and/or Cu-I cluster-centered transitions (^{3}CC).[29, 70] The lifetimes are on the same scale of previous reports on copper (I) iodide hybrids.[30, 71-73] The detailed fitting parameters are presented in **Table S26**. Among these four kinds of structures, compounds **6-9** with Cu_2I_2 rhomboid dimer or Cu_4I_4 cubane tetramer have relatively higher QY up to 67%. These results are consistent with prior studies that found compounds built on the Cu_2I_2 rhomboid dimer or Cu_4I_4 cubane tetramer tend to exhibit higher luminescence efficiency than those built on CuI chains.[74] This may result from the more condensed structures of the Cu_2I_2 rhomboid dimer or Cu_4I_4 cubane tetramer, which typically reduce nonradiative processes and thereby achieve higher quantum efficiencies. The higher condensation of Cu_2I_2 rhomboid dimer and Cu_4I_4 cubane tetramer structures **6-9** is indicated by their nearest centroid-to-centroid distance d_{cc} of inorganic motif (7.4-9.8 Å) as listed in **Table S27**, which is shorter than that (10.4-11.3 Å) for CuI chain structures **1-5**. The short d_{cc} (8.348 Å) for **10** indicates the high condensation of Cu_4I_4 octahedral tetramer structure. However, it has a low QY of 9 %, which may result from the luminescence quenching led by short ligand-ligand (3.48 Å) and Cu-Cu (2.158 Å) distance as a manifestation of the concentration-quenching effect. Moreover, it is interesting to notice that, within both Cu_2I_2 rhomboid dimer and Cu_4I_4 cubane tetramer structures, disordered compounds **1** and **7** have the highest luminescence efficiency. The higher capacity advantages of the disordered materials for applications in lithium battery have also been demonstrated, which is presumably associated with the more open lattice in the disordered framework that prevents the decomposition in some materials.[75] Although deeper analysis into the high luminescence efficiency of these disordered structures is beyond the scope of this work, it may be a worthwhile topic for researchers who are interested.

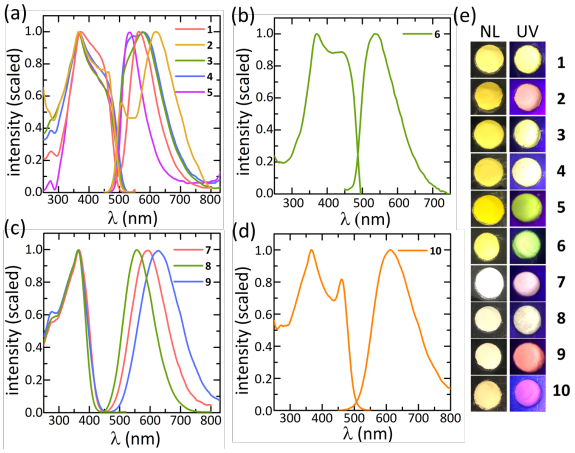

Figure 7. Photoluminescence excitation (PLE) and photoluminescence (PL) spectra of (a) CuI chain structures **1-5**, (b) Cu_2I_2 rhomboid dimer structure **6**, (c) Cu_4I_4 cubane tetramer structures **7-9**, and (d) Cu_4I_4 octahedral tetramer structure **10**. (e) Photographic images of the powder samples **1-10** under natural light (left) and 395 nm UV excitation (right).

It is also worth mentioning that the excitation performance of **7-9** is quite different with that of the other compounds. The PLE spectra of Cu_4I_4 cubane tetramer structures **7-9** manifest a sharp band peaking at 365 nm, which is significantly different from those of the other compounds, ranging from ultraviolet (UV) to blue light with two broad bands peaking at about 365 nm and 450 nm re-

Table 1. Bandgap, optimum excitation ($\lambda_{ex,\,max}$) and emission ($\lambda_{em,\,max}$) wavelengths, quantum yields (QY), and lifetimes of **1-10** at room temperature. *Represents the absorption onset of a pre-edge feature rather than the true bandgap.

Compounds	Bandgap (eV)	$\lambda_{ex,\,max}$ (nm)	$\lambda_{em,\,max}$ (nm)	FWHM (nm)	QY (%)	Lifetime (μs)
CuI(isoquinoline) (**1**)	2.61	370	560	100	30	3.4
CuI(3-methylisoquinoline)(**2**)	2.57	365	620	198	1	5.7
CuI(7-methylquinoline) (**3**)	2.56	365	575	150	12	1.8
CuI(3-methylquinoline) (**4**)	2.55	365	580	150	11	1.3
CuI(4-methylquinoline) (**5**)	2.48	365	530	78	5	0.5
$Cu_2I_2(Ph_3P)_2$(7-methylquinoline)$_2$ (**6**)	2.56	370	535	111	25	53.9
Cu_4I_4(2-methylpiperidine)$_4$ (**7**)	2.97	365	590	134	67	10.0
Cu_4I_4(4-methylpiperidine)$_4$ (**8**)	2.57*	365	555	112	65	11.3
Cu_4I_4(3,5-dimethylpiperidine)$_4$ (**9**)	2.89	365	625	156	20	2.4
Cu_4I_4(quinoline)$_4$ (**10**)	2.73	365	610	151	9	1.1

spectively. Since phosphors assembled with UV light emitting diodes (LEDs) and blue LEDs are two main configurations for efficient white light,[76, 77] exploring the excitation mechanism of copper iodide hybrids with different structures is of guiding importance for their potential applications. Based on the results of previous studies into the electronic transitions involved in the photoexcitation of copper iodide hybrids,[42, 78] combined with the theoretical investigations in this work, we find that the different excitation properties originate from the differences in electronic structure between copper iodide hybrids which incorporate aromatic (L_1-L_5, L_{10}) or aliphatic ligands (L_7-L_9), irrespective of the inorganic modules. Our calculations revealed that the HOMOs for the aromatic and aliphatic hybrids are similar, dominated by contributions from inorganic components (Cu 3d and I 5p), and thus culminate in as the singlet ground state S_0. Interestingly, the LUMOs are quite different. For aromatic hybrids (**1**-**6**, **10**) the LUMOs are mostly composed from the π* orbitals of the aromatic ligands with a combination of copper and iodine s-p states as the higher-lying unoccupied molecular orbitals. In contrast, in the aliphatic hybrids (**7**-**9**) the LUMOs are mainly comprised of inorganic components (I 5p) due to the lack of π* orbitals on aliphatic ligands. These results indicate that aromatic hybrids possess states from which low-energy excitations are possible, unlike their aliphatic counterparts. Consequently, in the former, blue-light excitation is possible, while in the latter, only higher energy UV radiation excites luminescence. These results demonstrate the great potential for copper (I) iodide hybrids in phosphor-converted LEDs (pc-LEDs). Specifically, the aromatic copper (I) iodide hybrids can be fabricated with either blue or UV LED chips, while the aliphatic copper (I) iodide hybrids can only be activated by UV LED chips.

To gain insight into the luminescence mechanism of copper (I) iodide hybrids with different inorganic motifs, the temperature-dependent PL spectra for the selected compounds of different structures were collected as shown in **Figure 8**. As the temperature decreases from 300 K to 2.8 K, the emission band of compound **8** with cubane tetramer structure displays a gradual red-shift from 560 nm to 590 nm, while that of compound **3** with 1D chain structure, **6** with rhomboid dimer structure, and **10** with octahedral tetramer structure displays a blue-shift and the discrete bands appear gradually. The sharp emission peak seen at 720 nm in all spectra is due to second order Rayleigh scattering from 360 nm excitation. The temperature-dependent spectra normalized at Rayleigh scattering peak 720 nm for these compounds are shown in Figure S4 to exhibit the absolute PL intensity change. The emission of copper iodide hybrids has been attributed to several different mechanisms, including metal to ligand charge transfer (MLCT), halide to ligand charge transfer (XLCT), and cluster-centered (CC) transitions involving halide to metal charge transfer (XMCT) and Cu (I) d^{10}-d^9s^1 metal centered transition, and sometimes a combination of these.[79] For compound **8** built of Cu_4I_4 cubane tetramer and aliphatic ligand, the emission appears to primarily originate from CC transitions - likely because both VBM and CBM are composed of inorganic atomic states due to the strong cuprophilic interaction. According to theoretical and experimental studies of copper iodide hybrids with dominant CC transitions,[80-83] the red-shift of emission upon cooling in compound **8** can be attributed to enhanced cuprophilic interactions due to shortening of the Cu-Cu distance at low temperature. As for compound **3**, **6**, and **10**, the blue-shift of the primary emission energy and appearance of multiple strong, narrow emission bands at low temperature can be attributed to a complex interplay between the three excited states for XLCT, MLCT and CC transition. According to Ford's work on the typical $Cu_4I_4(pyridine)_4$,[79] the low energy band can be ascribed to CC transition, and the high energy bands can be ascribed to (X+M)LCT. Since the CC excited state is thermally populated by (X+M)LCT,[30, 84] the relative intensity of emission from CC state decreases upon cooling, leading to the overall blue-shift in compound **3**, **6** and **10**. In the case of compound **3** and **6**, the shortest Cu-Cu distance is around or longer than the sum of the van der Waals radii (2.796 Å for **3**, 3.345 Å for **6**). We thus speculate that the CC emission in **3** and **6** predominantly arises from XMCT, due to weak cuprophilic interaction, therefore decreasing sensitivity to the contraction of the Cu-Cu cluster as the temperature decreases. It is interesting to notice that the emission spectra at low temperature for compound **10** present a sort of vibronic structure, as already observed for

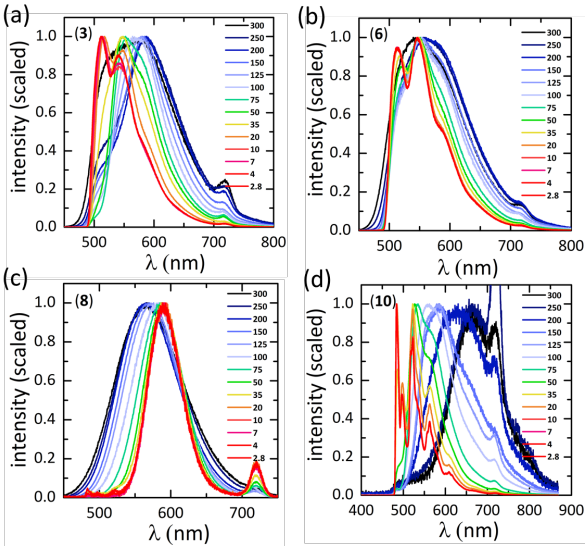

Figure 8. Temperature-dependent photoluminescence (PL) spectra of (a) CuI chain structure **3**, (b) Cu_2I_2 rhomboid dimer structure **6**, (c) Cu_4I_4 cubane tetramer structure **8**, and (d) Cu_4I_4 octahedral tetramer structure **10** recorded between 2.8 K and 300 K under 360 nm excitation.

$Cu_4I_4L_4$ (L=triphenylphosphine, tris(4-methoxyphenyl)phosphine, tris(4-tolyl)phosphine, l-phenyl-3,4-dimethylphosphole).[85-87] This can be attributed to vibration of the ligands due to its more rigid structure than the others (compound **3** and **6)** indicated by its shorter ligand-ligand distance (3.48 Å) and shorter centroid-to-centroid distance of inorganic motif (8.348).[87] In order to gain more information about the origin of the multi emission peaks at low temperature, the temperature-dependent lifetimes for these compounds of different structures were collected as shown in **Figure S5.** The lifetimes for all these compounds are gradually increasing with decreasing temperatures. The lifetimes of different emission bands for compound **10** are recorded separately as shown in **Figure S6**. They all show similar trends as temperature changes and approximate value at same temperature, which further indicate that these multi narrow emission bands could be attributed to the vibration of the organic ligands. Consequently, the emission of compound **8** with cubane tetramer structure is attributed to CC transitions, while the emission of **3** with 1D chain structure, **6** with rhomboid dimer structure, and **10** with octahedral tetramer is attributed to a combination of XLCT, MLCT and CC transition at room temperature, and dominated by XLCT and MLCT at low temperature.

CONCLUSIONS

We report the preparation of ten new hybrid copper (I) iodide phosphors with a diverse range of structural types including CuI 1D chain structures, Cu_2I_2 rhomboid dimer structures, Cu_4I_4 cubane tetramer structures, and octahedral Cu_4I_4 tetramer structures. The compounds emit in the useful, green-red region with QYs ranging from 1% to 67%. Among them, compounds with Cu_2I_2 rhomboid dimer or Cu_4I_4 cubane tetramer have relatively higher QY due to their more condensed inorganic motifs. DFT calculations have revealed the effects of the inorganic module and organic ligand on the electronic structures, demonstrating that the additional lower-lying unoccupied molecular orbitals from π* orbitals enable photoexcitation with blue, visible light of the copper iodide hybrids with aromatic ligands while those with aliphatic ligands require higher energy excitation. Based on the temperature dependent PL spectra for the selected compounds of different structures, we have systematically investigated the luminescence mechanism of the compounds with different inorganic motifs. We propose that the emission of compounds built of Cu_4I_4 cubane tetramer and aliphatic ligand is attributed to CC transitions, while the emission of compounds with 1D chain structure, rhomboid dimer structure, and octahedral tetramer is attributed to a combination of XLCT, MLCT and CC transition, and dominated by XLCT and MLCT at low temperature. This work expands the scope of copper (I) iodide hybrids, giving insight into their structural diversity and luminescence mechanisms, and also further improves our understanding of composition-structure-property correlations.

METHODS

Materials. CuI (98%, Sigma-Aldrich), isoquinoline (L_1, Spectrum Chemicals), 3-methylisoquinoline (L_2, 98%, Sigma-Aldrich), 7-methylquinoline (L_3, Spectrum Chemicals), 3-methylquinoline (L_4), 4-methylquinoline (L_5, Spectrum Chemicals), triphenylphosphine (L_6, Spectrum Chemicals), 2-methylpiperidine (L_7, 98%, Sigma-Aldrich), 4-methylpiperidine (L_8, 96%, Sigma-Aldrich), 3,5-dimethylpiperidine (L_9, 99%, Sigma-Aldrich), quinoline (L_{10}, Spectrum Chemicals), KI, acetonitrile were purchased from commercial sources and used as received.

Synthesis of 1-5. CuI (38 mg; 0.2 mmol) was dissolved in 5 mL acetonitrile, and 0.2 mmol A (A = isoquinoline, 3-methylquinoline, 7-methylquinoline, 3-methylquinoline, and 4-methylquinoline) dissolved in 2 mL acetonitrile was added to the above solution under heating at 82 ℃. The reaction mixture was kept heating for 1 min, and then allowed to cool to room temperature. Pale yellow needlelike crystals precipitated during slow cooling.

Synthesis of 6. CuI (47.5 mg; 0.25 mmol) was dissolved in a saturated aqueous KI solution (2 mL) which was placed in the reaction vial as the bottom layer. Ph_3P (131.1 mg; 0.5 mmol) and 7-methylquinoline (67.5 μL; 0.5 mmol) were dissolved in toluene (2 mL) as the top layer. The vial was kept closed at room temperature for 10 days to obtain pale yellow crystals.

Synthesis of 7-9. Single crystals of **7-9** were obtained by the layer method. CuI (95 mg; 0.5 mmol) was dissolved in a saturated aqueous KI solution (2 mL) which was placed in the reaction vial as the bottom layer. 2 mmol A (A = 2-methylpiperidine, 4-methylpiperidine, and 3,5-dimethylpiperidine) was dissolved in ethanol (2 cm^3) which was placed as the top layer. A mixture of ethanol (1 cm^3) and deionized water (1 cm^3) was used as the middle layer to separate the above solutions. The vial was kept closed at room temperature for 24 hours to obtain the colorless needlelike crystals.

Synthesis of 10. CuI (38 mg; 0.2 mmol) was dissolved in 5 mL acetonitrile, and 0.2 mmol quinoline dissolved in 2 mL acetonitrile was added to the above solution under heating at 82 ℃. The reaction mixture was kept heating for 1 min, and then allowed to cool to room temperature. Pale yellow needlelike crystals precipitated during slow cooling.

Single Crystal X-ray Diffraction (SCXRD) and Powder X-ray Diffraction (PXRD). SCXRD data were collected

using a Bruker KAPPA APEX II diffractometer equipped with an APEX II CCD detector using a TRIUMPH monochromator with an Mo Kα source (λ = 0.71073 Å) and MX Optics. SCXRD data for **2-6** and **8-9** were collected at room temperature, while that for the disordered structures **1**, **7** and **10** were collected at 100 K. Crystal structures were solved using direct methods and refined by full-matrix least-squares on F^2 using the SHELXL-2014 program package. PXRD patterns were collected using a PANalytical Empyrean powder diffractometer equipped with a Cu Kα radiation source (λ = 1.5418 Å).

Diffuse reflectance optical spectroscopy. Optical diffuse reflectance measurements were obtained using a Shimadzu UV3600 UV-NIR Spectrometer. Data were collected in the wavelength range of 220 nm to 800 nm using $BaSO_4$ as the reference of 100 % reflectance. The Kubelka-Munk function was used to convert the reflectance spectra to optical absorption.

Computational details. Density functional theory (DFT) calculations were performed using the Vienna Ab initio Simulation Package[88-90] (VASP), version 5.4.4. The Perdew-Burke-Ernzerhof[91] (PBE) functional and projector-augmented wave[92, 93] (PAW) pseudopotentials were used with a plane-wave cutoff energy of 1000 eV and energy convergence of 10^{-6} eV or better. PAW potentials were chosen following the version 5.2 guidelines. Automatic k-mesh generation was used with a length parameter (R_k) of 60. For band-structure calculations, an appropriate k-path was generated using SeeK-path[94, 95], and band-structures were plotted and analyzed using Sumo.[96, 97]

Photoluminescence, Internal Quantum Yield (QY), and Photoluminescence Lifetime Measurements. Photoluminescence emission (PL) and excitation (PLE) spectra, and QYs of powder samples were obtained on a Horiba FluoroMax-4 equipped with an integrating sphere using a 150 W continuous Xe arc lamp as excitation source. All the PL and PLE spectra were calibrated by built-in correction files. Photoluminescence lifetime (PLLT) measurements were performed using an in-house-built multiscaler analyzer setup. The excitation light pulses at 370 nm were generated by Light Conversions TOPAS Prime Optical Parametric Amplifier (OPA) with UV-Vis-NIR optical mixing unit. OPA was pumped with the output of Coherent Astrella femtosecond regenerative amplifier. The system produced ~160 femtosecond pulses with ~30 μJ energy with the repetition rate of 5 kHz. The laser pulses were attenuated with neutral density filters and focused on the sample. PL was collected and focused on the entrance slit of a monochromator (PI Acton SPC-300) by an imaging lens and the laser light was blocked by a long-pass interference filter (Omega Filters). The light dispersed by the monochromator was detected by a photon counting detector (Hamamatsu H8259-02). PL transients were recorded with Becker&Hickl MSA-300 multiscaler analyzer which was triggered by the Astrella timing electronics. Data were collected at room temperature.

Temperature-dependent Photoluminescence and Lifetime Measurements. Temperature-dependent photoluminescence (PL) spectra of powder samples were collected in a 4K closed-cycle cold-finger cryostat under a base pressure of 1×10^{-7} torr. Samples were photoexcited with 360 nm front-facing excitation, and this incident pulse was generated from the 800 nm output of a Ti:sapphire amplifier with 2kHz repetition rate and 35 fs pulse width using an optical parametric amplifier (OPA). The cryostat details for temperature-dependent lifetime measurements are the same as written above. Time-resolved photoluminescence measurements were collected using a streak-camera with front-facing photoexcitation. Photon counts for spectral and kinetic data were accumulated for 15 ms over 30,000 integrations of charge-coupled device (CCD) detector plate collections.

ASSOCIATED CONTENT

Crystallographic details, calculated and experimental X-ray diffraction patterns, DFT calculation results, and lifetime data. The Supporting Information is available free of charge via the Internet at http://pubs.acs.org.

AUTHOR INFORMATION

Corresponding Author

Ram Seshadri
Materials Department and Materials Research Laboratory, and Department of Chemistry and Biochemistry
University of California, Santa Barbara, California 93106, United States; orcid.org/0000-0001-5858-4027;
Email: seshadri@mrl.ucsb.edu

ACKNOWLEDGMENT

This work is supported by the U. S. Department of Energy, Office of Science, Basic Energy Sciences, under the grant DE-SC-0012541. We thank Anthony K. Cheetham for useful discussions. SW thanks the China Scholarship Council for a State Scholarship Fund. PV thanks the Science & Engineering Research Board (SERB) of the Govt. of India for Ramanujan Fellowship (Award No. RJF/2020/000106), and the Jawaharlal Nehru Centre for Advanced Scientific Research (JNCASR) Bangalore for financial support and research infrastructure. This work made use of the facilities of the Materials Research Science and Engineering Center (MRSEC) at UC Santa Barbara supported by the National Science Foundation (DMR 1720256). SMLT has been supported by the NSF Graduate Research Fellowship Program under Grant No. DGE- 1650114. SP has been supported by the NSF Graduate Research Fellowship Program under Grant No. DGE-1842165 and the Ryan Fellowship at Northwestern University. The ultrafast laser system used for the

PLLT measurements was funded by DURIP ARO grant 66886LSRIP. This work was performed, in part, at the Center for Nanoscale Materials, a U.S Department of Energy Office of Science User Facility, and supported by the U.S. Department of Energy, Office of Science, Office of Basic Energy Sciences, under Contract No. DE-AC02-06CH11357.

REFERENCES

1. Cheetham, A. K.; Rao, C.; Feller, R. K., Structural diversity and chemical trends in hybrid inorganic – organic framework materials. *Chem. Commun.* **2006**, (46), 4780-4795.
2. Gómez-Romero, P.; Sanchez, C., *Functional hybrid materials*. John Wiley & Sons: 2006.
3. Sanchez, C.; Shea, K. J.; Kitagawa, S., Recent progress in hybrid materials science. *Chemical Society Reviews* **2011,** 40, (2), 471-472.
4. Mao, L. L.; Stoumpos, C. C.; Kanatzidis, M. G., Two-Dimensional Hybrid Halide Perovskites: Principles and Promises. *J Am Chem Soc* **2019,** 141, (3), 1171-1190.
5. Sanchez, C.; Shea, K. J.; Kitagawa, S., Recent progress in hybrid materials science. *Chem. Soc. Rev.* **2011,** 40, (2), 471-472.
6. Jain, P.; Ramachandran, V.; Clark, R. J.; Zhou, H. D.; Toby, B. H.; Dalal, N. S.; Kroto, H. W.; Cheetham, A. K., Multiferroic behavior associated with an order – disorder hydrogen bonding transition in metal– organic frameworks (MOFs) with the perovskite ABX_3 architecture. *J. Am. Chem. Soc.* **2009,** 131, (38), 13625-13627.
7. Kagan, C. R.; Mitzi, D. B.; Dimitrakopoulos, C. D., Organic-inorganic hybrid materials as semiconducting channels in thin-film field-effect transistors. *Science* **1999,** 286, (5441), 945-947.
8. Smith, M. D.; Connor, B. A.; Karunadasa, H. I., Tuning the luminescence of layered halide perovskites. *Chem. Rev.* **2019,** 119, (5), 3104-3139.
9. Mao, L. l.; Guo, P. J.; Wang, S. X.; Cheetham, A. K.; Seshadri, R., Design principles for enhancing photoluminescence quantum yield in hybrid manganese bromides. *J. Am. Chem. Soc.* **2020,** 142, (31), 13582-13589.
10. Correa-Baena, J.-P.; Saliba, M.; Buonassisi, T.; Grätzel, M.; Abate, A.; Tress, W.; Hagfeldt, A., Promises and challenges of perovskite solar cells. *Science* **2017,** 358, (6364), 739-744.
11. Atodiresei, N.; Caciuc, V.; Lazić, P.; Blügel, S., Engineering the magnetic properties of hybrid organic-ferromagnetic interfaces by molecular chemical functionalization. *Phys. Rev. B.* **2011,** 84, (17), 172402.
12. Saines, P. J.; Melot, B. C.; Seshadri, R.; Cheetham, A. K., Synthesis, structure and magnetic phase transitions of the manganese succinate hybrid framework, $Mn(C_4H_4O_4)$. *Chem. - Eur. J.* **2010,** 16, (25), 7579-7585.
13. Vishnoi, P.; Zuo, J. L.; Strom, T. A.; Wu, G.; Wilson, S. D.; Seshadri, R.; Cheetham, A. K., Structural diversity and magnetic properties of hybrid ruthenium halide perovskites and related compounds. *Angew. Chem.* **2020,** 132, (23), 9059-9066.
14. Mao, L. L.; Guo, P. J.; Kepenekian, M.; Hadar, I.; Katan, C.; Even, J.; Schaller, R. D.; Stoumpos, C. C.; Kanatzidis, M. G., Structural Diversity in White-Light-Emitting Hybrid Lead Bromide Perovskites. *J Am Chem Soc* **2018,** 140, (40), 13078-13088.
15. Saparov, B.; Mitzi, D. B., Organic–inorganic perovskites: structural versatility for functional materials design. *Chem. Rev.* **2016,** 116, (7), 4558-4596.
16. Dolbecq, A.; Dumas, E.; Mayer, C. R.; Mialane, P., Hybrid organic– inorganic polyoxometalate compounds: from structural diversity to applications. *Chem. Rev.* **2010,** 110, (10), 6009-6048.
17. Furman, J. D.; Warner, A. Y.; Teat, S. J.; Mikhailovsky, A. A.; Cheetham, A. K., Tunable, ligand-based emission from inorganic– organic frameworks: a new approach to phosphors for solid state lighting and other applications. *Chem. Mater.* **2010,** 22, (7), 2255-2260.
18. Smith, M. D.; Crace, E. J.; Jaffe, A.; Karunadasa, H. I., The diversity of layered halide perovskites. *Annu. Rev. Mater. Res.* **2018,** 48, 111-136.
19. Liu, W.; Lustig, W. P.; Li, J., Luminescent inorganic-organic hybrid semiconductor materials for energy-saving lighting applications. *EnergyChem* **2019,** 1, (2), 100008.
20. Dohner, E. R.; Jaffe, A.; Bradshaw, L. R.; Karunadasa, H. I., Intrinsic white-light emission from layered hybrid perovskites. *J. Am. Chem. Soc.* **2014,** 136, (38), 13154-13157.
21. Zhang, L.; Yang, X.; Jiang, Q.; Wang, P.; Yin, Z.; Zhang, X.; Tan, H.; Yang, Y. M.; Wei, M.; Sutherland, B. R., Ultra-bright and highly efficient inorganic based perovskite light-emitting diodes. *Nat. Commun.* **2017,** 8, (1), 1-8.
22. Yangui, A.; Roccanova, R.; Wu, Y.; Du, M.-H.; Saparov, B., Highly efficient broad-band luminescence involving organic and inorganic molecules in a zero-dimensional hybrid lead chloride. *J. Phys. Chem. C.* **2019,** 123, (36), 22470-22477.
23. Mao, L.; Wu, Y.; Stoumpos, C. C.; Traore, B.; Katan, C.; Even, J.; Wasielewski, M. R.; Kanatzidis, M. G., Tunable White-Light Emission in Single-Cation-Templated Three-Layered 2D Perovskites $(CH_3CH_2NH_3)_4Pb_3Br_{10-x}Cl_x$. *J. Am. Chem. Soc.* **2017,** 139, (34), 11956-11963.

24. Liu, W.; Fang, Y.; Li, J., Copper Iodide Based Hybrid Phosphors for Energy-Efficient General Lighting Technologies. *Adv. Funct. Mater.* **2018,** 28, (8), 1705593.
25. Zhu, K.; Cheng, Z.; Rangan, S.; Cotlet, M.; Du, J.; Kasaei, L.; Teat, S. J.; Liu, W.; Chen, Y.; Feldman, L. C., A New Type of Hybrid Copper Iodide as Nontoxic and Ultrastable LED Emissive Layer Material. *ACS Energy Lett.* **2021,** 6, 2565-2574.
26. Peng, R.; Li, M.; Li, D., Copper(I) halides: A versatile family in coordination chemistry and crystal engineering. *Coordin. Chem. Rev.* **2010,** 254, (1-2), 1-18.
27. Cariati, E.; Roberto, D.; Ugo, R.; Ford, P. C.; Galli, S.; Sironi, A., X-ray Structures and Emissive and Second-Order Nonlinear Optical Properties of Two Inorganic– Organic Polymeric Adducts of CuI with 4-Acetylpyridine. The Role of Both "Intrastrand" Charge Transfers and Structural Motifs on the Nonlinear Optical Response of Cu (I) Polymeric Adducts with Pseudoaromatic η^1-Nitrogen Donor Ligands. *Chem. Mater.* **2002,** 14, (12), 5116-5123.
28. Ford, P. C.; Cariati, E.; Bourassa, J., Photoluminescence properties of multinuclear copper (I) compounds. *Chem. Rev.* **1999,** 99, (12), 3625-3647.
29. Mazzeo, P. P.; Maini, L.; Petrolati, A.; Fattori, V.; Shankland, K.; Braga, D., Phosphorescence quantum yield enhanced by intermolecular hydrogen bonds in Cu_4I_4 clusters in the solid state. *Dalton Trans.* **2014,** 43, (25), 9448-55.
30. Farinella, F.; Maini, L.; Mazzeo, P.; Fattori, V.; Monti, F.; Braga, D., White luminescence achieved by a multiple thermochromic emission in a hybrid organic–inorganic compound based on 3-picolylamine and copper (I) iodide. *Dalton Trans.* **2016,** 45, (44), 17939-17947.
31. Hou, F.; Powell, M.; Dougherty, D. B.; Sommer, R. D.; Maggard, P. A., Tunable Optical and Photocatalytic Properties of Low-Dimensional Copper (I)-Iodide Hybrids Using Coordinating Organic Ligands. *Cryst. Growth Des.* **2018,** 18, (9), 5406-5416.
32. Safko, J. P.; Kuperstock, J. E.; McCullough, S. M.; Noviello, A. M.; Li, X.; Killarney, J. P.; Murphy, C.; Patterson, H. H.; Bayse, C. A.; Pike, R. D., Network formation and photoluminescence in copper(I) halide complexes with substituted piperazine ligands. *Dalton Trans.* **2012,** 41, (38), 11663-74.
33. Li, J.-C.; Li, H.-X.; Li, H.-Y.; Gong, W.-J.; Lang, J.-P., Ligand coordination site-directed assembly of copper (I) iodide complexes of ((pyridyl)-1-pyrazolyl) pyridine. *Cryst. Growth Des.* **2016,** 16, (3), 1617-1625.
34. Ohara, H.; Kobayashi, A.; Kato, M., Simple and extremely efficient blue emitters based on mononuclear Cu (I)-halide complexes with delayed fluorescence. *Dalton Trans.* **2014,** 43, (46), 17317-17323.
35. Chen, J.-L.; Song, P.; Liao, J.; Wen, H.-R.; Hong, R.; Chen, Z.-N.; Chi, Y., Luminescent homodinuclear copper (I) halide complexes based on the 3, 5-bis {6-(2, 2′ -dipyridyl)} pyrazole ligand. *Inorg. Chem. Commun.* **2010,** 13, (9), 1057-1060.
36. Aguirrechu-Comerón, A.; Hernandez-Molina, R.; Rodriguez-Hernandez, P.; Munoz, A.; Rodriguez-Mendoza, U. R.; Lavín, V. c.; Angel, R. J.; Gonzalez-Platas, J., Experimental and ab initio study of catena (bis (μ_2-iodo)-6-methylquinoline-copper (i)) under pressure: synthesis, crystal structure, electronic, and luminescence properties. *Inorg. chem.* **2016,** 55, (15), 7476-7484.
37. Kitada, N.; Ishida, T., Polymeric one-and two-dimensional copper (I) iodide complexes showing photoluminescence tunable by azaaromatic ligands. *CrystEngComm* **2014,** 16, (34), 8035-8040.
38. Zhang, X.; Liu, W.; Wei, G. Z.; Banerjee, D.; Hu, Z.; Li, J., Systematic approach in designing rare-Earth-free hybrid semiconductor phosphors for general lighting applications. *J. Am. Chem. Soc.* **2014,** 136, (40), 14230-6.
39. Liu, W.; Fang, Y.; Wei, G. Z.; Teat, S. J.; Xiong, K.; Hu, Z.; Lustig, W. P.; Li, J., A Family of Highly Efficient CuI-Based Lighting Phosphors Prepared by a Systematic, Bottom-up Synthetic Approach. *J Am Chem Soc* **2015,** 137, (29), 9400-8.
40. Wang, S. X.; Morgan, E. E.; Vishnoi, P.; Mao, L. L.; Teicher, S. M.; Wu, G.; Liu, Q. L.; Cheetham, A. K.; Seshadri, R., Tunable Luminescence in Hybrid Cu (I) and Ag (I) Iodides. *Inorg. Chem.* **2020,** 59, (20), 15487-15494.
41. Mondal, R.; Lozada, I. B.; Davis, R. L.; Williams, J. G.; Herbert, D. E., Site-selective benzannulation of N-heterocycles in bidentate ligands leads to blue-shifted emission from $[(P\text{^}N)Cu]_2(\mu\text{-}X)_2$ dimers. *Inorg. Chem.* **2018,** 57, (9), 4966-4978.
42. Fang, Y.; Liu, W.; Teat, S. J.; Dey, G.; Shen, Z.; An, L.; Yu, D.; Wang, L.; O'Carroll, D. M.; Li, J., A Systematic Approach to Achieving High Performance Hybrid Lighting Phosphors with Excellent Thermal - and Photostability. *Adv. Funct. Mater.* **2017,** 27, (3), 1603444.
43. Xie, M. C.; Han, C. M.; Zhang, J.; Xie, G. H.; Xu, H., White electroluminescent phosphine-chelated copper iodide nanoclusters. *Chem. Mater.* **2017,** 29, (16), 6606-6610.
44. Hou, Q.; Jia, M.-J.; Zhao, J.-J.; Jin, J.; Yu, J.-H.; Xu, J.-Q., Two new 3-D photoluminescence metal–organic frameworks based on cubane Cu_4I_4 clusters as tetrahedral nodes. *Inorg. Chim. Acta.* **2012,** 384, 287-292.
45. Fu, W. F.; Gan, X.; Che, C. M.; Cao, Q. Y.; Zhou, Z. Y.; Zhu, N. N. Y., Cuprophilic interactions in

luminescent copper (I) clusters with bridging bis (dicyclohexylphosphino) methane and iodide ligands: spectroscopic and structural investigations. *Chem. Eur. J.* **2004,** 10, (9), 2228-2236.
46. Chen, B.-L.; Mok, K.-F.; Ng, S.-C., Synthesis, crystal structures and dynamic NMR studies of novel trinuclear copper (I) halide complexes with 2, 5-bis [(diphenylphosphino) methyl] thiophene. *J. Chem. Soc. Dalton Trans.* **1998**, (17), 2861-2866.
47. Yu, Y.-D.; Meng, L.-B.; Chen, Q.-C.; Chen, G.-H.; Huang, X.-C., Substituent regulated photoluminescent thermochromism in a rare type of octahedral Cu_4I_4 clusters. *New J. Chem.* **2018,** 42, (11), 8426-8437.
48. Musina, E.; Shamsieva, A.; Strelnik, I.; Gerasimova, T.; Krivolapov, D.; Kolesnikov, I.; Grachova, E.; Tunik, S.; Bannwarth, C.; Grimme, S., Synthesis of novel pyridyl containing phospholanes and their polynuclear luminescent copper (I) complexes. *Dalton Trans.* **2016,** 45, (5), 2250-2260.
49. Chen, K.; Shearer, J.; Catalano, V. J., Subtle modulation of $Cu_4X_4L_2$ phosphine cluster cores leads to changes in luminescence. *Inorg. Chem.* **2015,** 54, (13), 6245-6256.
50. Benito, Q.; Le Goff, X. F.; Nocton, G.; Fargues, A.; Garcia, A.; Berhault, A.; Kahlal, S.; Saillard, J.-Y.; Martineau, C.; Trébosc, J., Geometry flexibility of copper iodide clusters: variability in luminescence thermochromism. *Inorg. Chem.* **2015,** 54, (9), 4483-4494.
51. Ohi, H.; Tachi, Y.; Kunimoto, T.; Itoh, S., Structure and photoluminescence property of two-dimensional coordination polymer complexes involving $Cu(I)_6X_6$ (X= Cl, Br, I) hexagon prism cluster supported by a tripodal tripyridine ligand with 1, 3, 5-triethylbenzene spacer. *Dalton Trans.* **2005**, (19), 3146-3147.
52. Amoore, J. J.; Hanton, L. R.; Spicer, M. D., Banded ribbons of Cu_6I_6 hexamers and multimodal thioether pyrazine ligands linked by self-complementary N··· H–C synthons. *Dalton Trans.* **2003**, (6), 1056-1058.
53. Liu, Z.; Djurovich, P. I.; Whited, M. T.; Thompson, M. E., Cu_4I_4 clusters supported by P∧N-type ligands: new structures with tunable emission colors. *Inorg. Chem.* **2012,** 51, (1), 230-236.
54. Maini, L.; Mazzeo, P. P.; Farinella, F.; Fattori, V.; Braga, D., Mechanochemical preparation of copper iodide clusters of interest for luminescent devices. *Faraday discuss.* **2014,** 170, 93-107.
55. Naik, S.; Mague, J. T.; Balakrishna, M. S., Short-Bite PNP Ligand-Supported Rare Tetranuclear $[Cu_4I_4]$ Clusters: Structural and Photoluminescence Studies. *Inorg. Chem.* **2014,** 53, (7), 3864-3873.
56. Emerson, E. W.; Cain, M. F.; Sanderson, M. D.; Knarr, C. B.; Glueck, D. S.; Ahern, J. C.; Patterson, H. E.; Rheingold, A. L., Synthesis, structure, and luminescence of the "octahedral" cluster Cu_4I_4(rac-$IsMePCH_2PMeIs)_2$(Is= 2, 4, 6-(i-Pr)$_3C_6H_2$). *Inorg. Chim. Acta.* **2015,** 427, 168-172.
57. Ahuja, R.; Nethaji, M.; Samuelson, A. G., Chelating and bridging bis (diphenylphosphino) aniline complexes of copper (I). *Inorg. Chim. Acta.* **2011,** 372, (1), 220-226.
58. Mézailles, N.; Le Floch, P.; Waschbüsch, K.; Ricard, L.; Mathey, F.; Kubiak, C. P., Synthesis and X-ray crystal structures of dimeric nickel (0) and tetrameric copper (I) iodide complexes of 2-diphenylphosphino-3-methylphosphinine. *J. Organomet. Chem.* **1997,** 541, (1-2), 277-283.
59. Marsich, N.; Nardin, G.; Randaccio, L., Tetranuclear copper (I) complex. Crystal and molecular structure of the 2:1 derivative of copper (I) iodide and bis (diphenylphosphino) methane. *J. Am. Chem. Soc.* **1973,** 95, (12), 4053-4054.
60. Daly, S.; Haddow, M. F.; Orpen, A. G.; Rolls, G. T.; Wass, D. F.; Wingad, R. L., Copper (I) Diphosphine Catalysts for C–N Bond Formation: Synthesis, Structure, and Ligand Effects. *Organometallics* **2008,** 27, (13), 3196-3202.
61. Zink, D. M.; Grab, T.; Baumann, T.; Nieger, M.; Barnes, E. C.; Klopper, W.; Bräse, S., Experimental and theoretical study of novel luminescent di-, tri-, and tetranuclear copper triazole complexes. *Organometallics* **2011,** 30, (12), 3275-3283.
62. Scherer, M.; Stein, D.; Breher, F.; Geier, J.; Schönberg, H.; Grützmacher, H., Copper (I) Chloride Cluster Complexes with Pentaphenyl - Cyclopentaphosphane as Ligand. *Z. Anorg. Allg. Chem.* **2005,** 631, (13 - 14), 2770-2774.
63. Ki, W.; Hei, X.; Yi, H. T.; Liu, W.; Teat, S. J.; Li, M.; Fang, Y.; Podzorov, V.; Garfunkel, E.; Li, J., Two-Dimensional Copper Iodide-Based Inorganic–Organic Hybrid Semiconductors: Synthesis, Structures, and Optical and Transport Properties. *Chem. Mater.* **2021,** 33, (13), 5317-5325.
64. Jeß, I.; Taborsky, P.; Pospíšil, J.; Näther, C., Synthesis, crystal structure, thermal and luminescence properties of CuX (2, 3-dimethylpyrazine) (X= Cl, Br, I) coordination polymers. *Dalton Trans.* **2007**, (22), 2263-2270.
65. Hu, S.; Zhang, Z.-M.; Meng, Z.-S.; Lin, Z.-J.; Tong, M.-L., Anion-dependent construction of copper (I/II)-1, 2, 4, 5-tetra (4-pyridyl) benzene frameworks. *CrystEngComm* **2010,** 12, (12), 4378-4385.
66. Yang, X.-J.; Li, H.-X.; Xu, Z.-L.; Li, H.-Y.; Ren, Z.-G.; Lang, J.-P., Spacer length-controlled assembly of

[Cu_nI_n]-based coordination polymers from CuI and bis (4-phenylpyrimidine-2-thio) alkane ligands. *CrystEngComm* **2012,** 14, (5), 1641-1652.
67. Zink, D. M.; Bächle, M.; Baumann, T.; Nieger, M.; Kühn, M.; Wang, C.; Klopper, W.; Monkowius, U.; Hofbeck, T.; Yersin, H., Synthesis, structure, and characterization of dinuclear copper (I) halide complexes with P^N ligands featuring exciting photoluminescence properties. *Inorg. Chem.* **2013,** 52, (5), 2292-2305.
68. Wang, R.-Y.; Zhang, X.; Yu, J.-H.; Xu, J.-Q., Copper (I)–polymers and their photoluminescence thermochromism properties. *Photochem. Photobiol. Sci.* **2019,** 18, (2), 477-486.
69. Rath, N. P.; Holt, E. M.; Tanimura, K., Fluorescent copper (I) complexes: Structural and spectroscopic characterization of bis (p-toluidine) bis (acetonitrile) tetraiodotetracopper and bis [(p-chloroaniline)(acetonitrile) diiododicopper] tetrameric complexes of mixed-ligand character. *Inorg. Chem.* **1985,** 24, (23), 3934-3938.
70. Nagaoka, S.; Ozawa, Y.; Toriumi, K.; Abe, M., A Dual-emission strategy for a wide-range phosphorescent color-tuning of a crystalline-state molecular cluster [Cu_4I_4(2-Bzpy)$_4$] (2-Bzpy = 2-Benzylpyridine). *Chem. Lett.* **2018,** 47, (9), 1101-1104.
71. Zhan, S.-Z.; Li, M.; Zheng, J.; Wang, Q.-J.; Ng, S. W.; Li, D., Luminescent Cu_4I_4–Cu_3(Pyrazolate)$_3$ Coordination Frameworks: Postsynthetic Ligand Substitution Leads to Network Displacement and Entanglement. *Inorg. Chem.* **2017,** 56, (21), 13446-13455.
72. Khatri, N. M.; Pablico-Lansigan, M. H.; Boncher, W. L.; Mertzman, J. E.; Labatete, A. C.; Grande, L. M.; Wunder, D.; Prushan, M. J.; Zhang, W.; Halasyamani, P. S.; Monteiro, J. H.; Bettencourt-Dias, A.; Stoll, S. L., Luminescence and Nonlinear Optical Properties in Copper(I) Halide Extended Networks. *Inorg Chem* **2016,** 55, (21), 11408-11417.
73. Xu, C.; Lv, L.; Luo, D.; Liu, W., Synthesis, structure and photoluminescence properties of three copper (i) iodide based inorganic–organic hybrid structures with pyrazine derivatives. *New J. Chem.* **2020,** 44, (33), 14103-14107.
74. Liu, W.; Zhu, K.; Teat, S. J.; Dey, G.; Shen, Z.; Wang, L.; O'Carroll, D. M.; Li, J., All-in-One: Achieving Robust, Strongly Luminescent and Highly Dispersible Hybrid Materials by Combining Ionic and Coordinate Bonds in Molecular Crystals. *J Am Chem Soc* **2017,** 139, (27), 9281-9290.
75. Julien, C.; Mauger, A.; Vijh, A.; Zaghib, K., Lithium batteries. In *Lithium Batteries*, Springer: 2016; pp 295-322.
76. Xia, Z. G.; Liu, Q. L., Progress in discovery and structural design of color conversion phosphors for LEDs. *Prog. Mater. Sci.* **2016,** 84, 59-117.
77. George, N. C.; Denault, K. A.; Seshadri, R., Phosphors for solid-state white lighting. *Annu. Rev. Mater. Res.* **2013,** 43, 481-501.
78. Currie, E.; King, B.; Lawrenson, A. L.; Schroeder, L. K., Electronic transitions involved in the absorption spectrum and dual luminescence of tetranuclear cubane [Cu_4I_4(pyridine)$_4$] cluster: a density functional theory/time-dependent density functional theory investigation. *Inorg. Chem.* **2006,** 45, (26), 10576-84.
79. Vitale, M.; Palke, W. E.; Ford, P. C., Origins of the double emission of the tetranuclear copper (I) cluster Cu_4I_4 (pyridine)$_4$: An ab initio study. *J. Phys. Chem.* **1992,** 96, (21), 8329-8336.
80. Kitagawa H; Ozawa Y; Toriumi K, Flexibility of cubane-like Cu_4I_4 framework: temperature dependence of molecular structure and luminescence thermochromism of [Cu_4I_4(PPh_3)$_4$] in two polymorphic crystalline states. *Chem. Commun.* **2010,** 46, 6302-6304.
81. Kim, T.; Shin, Y.; Jung, J.; Kim, J.; Kim, J., Crystal-to-Crystal Transformation between Three CuI Coordination Polymers and Structural Evidence for Luminescence Thermochromism. *Angew. Chem.* **2008,** 120, 697-700.
82. Sun, D.; Yuan, S.; Wang, H.; Lu, H. F.; Feng, S. Y.; Sun, D. F., Luminescence thermochromism of two entangled copper-iodide networks with a large temperature dependent emission shift. *Chem. Commun.* **2013,** 49, 6152-6154.
83. Maini, L.; Braga, D.; Mazzeo, P. P.; Ventura, B., Polymorph and isomer conversion of complexes based on CuI and PPh_3 easily observed via luminescence. *Dalton Trans.* **2012,** 41, (2), 531-539.
84. Ryu, C. K.; Vitale, M.; Ford, P. C., Photoluminescence properties of the structurally analogous tetranuclear copper (I) clusters Cu_4X_4 (dpmp)$_4$ (X= I, Br, Cl; dpmp= 2-(diphenylmethyl)pyridine). *Inorg. Chem.* **1993,** 32, (6), 869-874.
85. Perruchas, S.; Tard, C.; Le Goff, X. F.; Fargues, A.; Garcia, A.; Kahlal, S.; Saillard, J.-Y.; Gacoin, T.; Boilot, J.-P., Thermochromic luminescence of copper iodide clusters: The case of phosphine ligands. *Inorg. Chem.* **2011,** 50, (21), 10682-10692.
86. Huitorel, B.; El Moll, H.; Utrera-Melero, R.; Cordier, M.; Fargues, A.; Garcia, A.; Massuyeau, F.; Martineau-Corcos, C.; Fayon, F.; Rakhmatullin, A., Evaluation of ligands effect on the photophysical properties of copper iodide clusters. *Inorg. Chem.* **2018,** 57, (8), 4328-4339.

87. Lai, D. C.; Zink, J. I., Vibronic structure in the emission spectrum of the tetranuclear copper cluster $[Cu_4I_4(dmpp)_4]$. *Inorg. Chem.* **1993,** 32, (11), 2594-2596.
88. Kresse, G.; Furthmüller, J., Efficiency of ab-initio total energy calculations for metals and semiconductors using a plane-wave basis set. *Comput. Mater. Sci.* **1996,** 6, (1), 15-50.
89. Kresse, G.; Hafner, J., Ab initio molecular-dynamics simulation of the liquid-metal–amorphous-semiconductor transition in germanium. *Phys. Rev. B* **1994,** 49, (20), 14251-14269.
90. Kresse, G.; Furthmüller, J., Efficient iterative schemes for ab initio total-energy calculations using a plane-wave basis set. *Phys. Rev. B* **1996,** 54, (16), 11169-11186.
91. Perdew, J. P.; Burke, K.; Ernzerhof, M., Generalized gradient approximation made simple. *Phys. Rev. Lett.* **1996,** 77, (18), 3865-3868.
92. Blöchl, P. E., Projector augmented-wave method. *Phys. Rev. B* **1994,** 50, (24), 17953-17979.
93. Kresse, G.; Joubert, D., From ultrasoft pseudopotentials to the projector augmented-wave method. *Phys. Rev. B.* **1999,** 59, (3), 1758-1775.
94. Hinuma, Y.; Pizzi, G.; Kumagai, Y.; Oba, F.; Tanaka, I., Band structure diagram paths based on crystallography. *Comput. Mater. Sci.* **2017,** 128, 140-184.
95. Togo, A.; Tanaka, I., Spglib: a software library for crystal symmetry search. *arXiv preprint arXiv:1808.01590* **2018**.
96. Ganose, A. M.; Jackson, A. J.; Scanlon, D. O., Sumo: Command-line tools for plotting and analysis of periodic* ab initio* calculations. *J. Open Source Softw.* **2018,** 3, (28), 717.
97. Ong, S. P.; Richards, W. D.; Jain, A.; Hautier, G.; Kocher, M.; Cholia, S.; Gunter, D.; Chevrier, V. L.; Persson, K. A.; Ceder, G., Python Materials Genomics (pymatgen): A robust, open-source python library for materials analysis. *Comput. Mater. Sci.* **2013,** 68, 314-319.

Graphic for Table of Contents

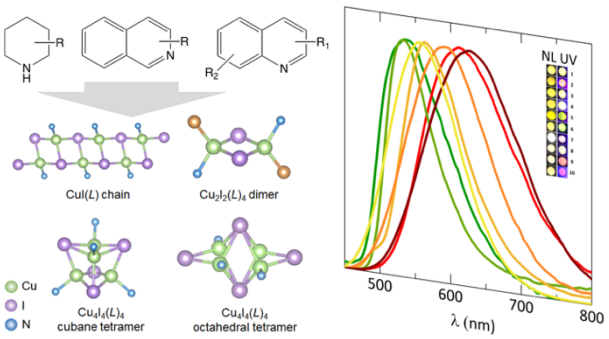

Supporting Information for

Ligand Control of Structural Diversity in Luminescent Hybrid Copper (I) Iodides

Shuxin Wang,[1,2] Emily E. Morgan,[1] Shobhana Panuganti,[3] Lingling Mao,[4] Pratap Vishnoi,[5] Guang Wu,[6] Quanlin Liu,[2] Mercouri G. Kanatzidis,[3,7] Richard D. Schaller,[3,8] Ram Seshadri[1,6]*

[1]Materials Department and Materials Research Laboratory
University of California, Santa Barbara, California 93106, United States

[2]The Beijing Municipal Key Laboratory of New Energy Materials and Technologies,
School of Materials Sciences and Engineering
University of Science and Technology Beijing, Beijing 100083, China

[3]Department of Chemistry
Northwestern University, Evanston, Illinois 60208, United States

[4]Department of Chemistry, Southern University of Science and Technology, Guangdong Shenzhen, 518055 China

5 New Chemistry Unit & International Centre for Materials Science, Jawaharlal Nehru Centre for Advanced Scientific Research, New Chemistry Unit, Jakkur, Bangalore, 560064 India

[6]Department of Chemistry and Biochemistry
University of California Santa Barbara, California 93106, United States

[7]Material Science Division
Argonne National Laboratory, Lemont, Illinois 60439, United States

[8]Center for Nanoscale Materials
Argonne National Laboratory, Lemont, Illinois 60439, United States

Table of contents

Section S1. Crystallographic details.

Table S1 Crystallographic and Structural Refinements Details for **1-5**.

Compounds	CuI(isoquinoline) (**1**)	CuI(3-methylisoquinoline) (**2**)	CuI(7-methylquinoline) (**3**)
Empirical formula	C_9H_7CuIN	$C_{10}H_{10}CuIN$	$C_{10}H_9CuIN$
Formula weight	319.60	334.63	333.62
Temperature	100(2) K	299(2) K	289(2) K
Wavelength	0.71073 Å	0.71073 Å	0.71073 Å
Crystal system	monoclinic	orthorhombic	monoclinic
Space group	P 21/m	P c a 21	P 21/c
Unit cell dimensions	a = 10.422(3) Å b = 4.1864(11) Å c = 11.767(3) Å α = 90° β = 115.696(6)° γ = 90°	a = 32.967(18) Å b = 4.200(2) Å c = 14.942(8) Å α = 90° β = 90° γ = 90°	a = 4.262(7) Å b = 18.28(3) Å c = 13.52(2) Å α = 90° β = 95.76(3)° γ = 90°
Volume	462.7(2) $Å^3$	2069(2) $Å^3$	1048(3) $Å^3$
Z	2	8	4
Density (calculated)	2.294 g/cm^3	2.149 g/cm^3	2.114 g/cm^3
Absorption coefficient	5.636 mm^{-1}	5.047 mm^{-1}	4.980 mm^{-1}
F(000)	300	1272	632
Crystal size	0.300 x 0.050 x 0.050 mm^3	0.250 x 0.050 x 0.050 mm^3	0.300 x 0.050 x 0.050 mm^3
θ range for data collection	1.921 to 26.407°	1.235 to 25.347°	1.879 to 25.782°
Reflections collected	3355	9132	5495
Independent reflections	1081 [R_{int} = 0.0388]	3714 [R_{int} = 0.0462]	1937 [R_{int} = 0.1087]
Completeness to θ = 25.242°	99.6%	100%	97.7%
Refinement method	Full-matrix least-squares on F^2	Full-matrix least-squares on F^2	Full-matrix least-squares on F^2
Data / restraints / parameters	1081 / 90 / 113	3714 / 1 / 238	1937 / 0 / 114
Goodness-of-fit	1.239	1.082	1.195
Final R indices [I > 2σ(I)]	R_{obs} = 0.0378, wR_{obs} = 0.1357	R_{obs} = 0.0532, wR_{obs} = 0.1305	R_{obs} = 0.1360, wR_{obs} = 0.3078
R indices [all data]	R_{all} = 0.0435, wR_{all} = 0.1383	R_{all} = 0.0665, wR_{all} = 0.1411	R_{all} = 0.1708, wR_{all} = 0.3237
Largest diff. peak and hole	1.198 and -0.885 $e·Å^{-3}$	3.488 and -0.918 $e·Å^{-3}$	3.846 and -2.257 $e·Å^{-3}$

Compounds	CuI(3-methylquinoline) (**4**)	CuI(4-methylquinoline) (**5**)
Empirical formula	$C_{10}H_9CuIN$	$C_{10}H_9CuIN$

Formula weight	333.62	333.62
Temperature	289(2) K	289(2) K
Wavelength	0.71073 Å	0.71073 Å
Crystal system	monoclinic	monoclinic
Space group	P 21/n	C 2/c
Unit cell dimensions	a = 4.192(3) Å b = 15.772(10) Å c = 15.612(9) Å α = 90° β = 95.885(16)° γ = 90°	a = 21.12(6) Å b = 4.208(12) Å c = 22.91(7) Å α = 90° β = 101.27(3)° γ = 90°
Volume	1026.8(11) $Å^3$	1997(10) $Å^3$
Z	4	8
Density (calculated)	2.158 g/cm^3	2.219 g/cm^3
Absorption coefficient	5.084 mm^{-1}	5.228 mm^{-1}
F(000)	632	1264
Crystal size	0.25 x 0.05 x 0.05 mm^3	0.200 x 0.050 x 0.050 mm^3
θ range for data collection	1.840 to 25.791°	1.813 to 25.680°
Reflections collected	1881	4287
Independent reflections	1881 [R_{int} = 0.0934]	1875 [R_{int} = 0.0983]
Completeness to θ = 25.242°	96.2%	99.3%
Refinement method	Full-matrix least-squares on F^2	Full-matrix least-squares on F^2
Data / restraints / parameters	1881 / 0 / 71	1875 / 1 / 83
Goodness-of-fit	1.059	1.369
Final R indices [I > 2σ(I)]	R_{obs} = 0.1214, wR_{obs} = 0.2434	R_{obs} = 0.0736, wR_{obs} = 0.1127
R indices [all data]	R_{all} = 0.2235, wR_{all} = 0.2785	R_{all} = 0.1395, wR_{all} = 0.1231
Largest diff. peak and hole	1.670 and -1.495 e·$Å^{-3}$	1.835 and -1.268 e·$Å^{-3}$

Table S2. Crystallographic and Structural Refinements Details for **6**.

Compounds	$Cu_2I_2(Ph_3P)_2$(7-methylquinoline)$_2$ (**6**)
Empirical formula	$C_{28}H_{24}CuINP$
Formula weight	595.89
Temperature	298(2) K
Wavelength	0.71073 Å
Crystal system	triclinic
Space group	P -1
Unit cell dimensions	a = 9.764(6) Å b = 10.578(7) Å

	c = 13.342(9) Å
	α = 71.223(18)°
	β = 74.200(16)°
	γ = 86.19(3)°
Volume	1255.0(14) $Å^3$
Z	2
Density (calculated)	1.577 g/cm^3
Absorption coefficient	2.180 mm^{-1}
F(000)	592
Crystal size	0.200 x 0.150 x 0.100 mm^3
θ range for data collection	1.672 to 25.681°
Reflections collected	9755
Independent reflections	4760 [R_{int} = 0.0207]
Completeness to θ = 25.242°	100%
Refinement method	Full-matrix least-squares on F^2
Data / restraints / parameters	4760 / 0 / 290
Goodness-of-fit	1.035
Final R indices [I > 2σ(I)]	R_{obs} = 0.0287, wR_{obs} = 0.0685
R indices [all data]	R_{all} = 0.0361, wR_{all} = 0.0727
Largest diff. peak and hole	0.842 and -0.393 e·$Å^{-3}$

Table S3. Crystallographic and Structural Refinements Details for **7-9**.

Compounds	Cu_4I_4(2-methylpiperidine)$_4$ (**7**)	Cu_4I_4(4-methylpiperidine)$_4$ (**8**)	Cu_4I_4(3,5-dimethylpiperidine)$_4$ (**9**)
Empirical formula	C_7HCuIN	$C_{24}H_{52}Cu_4I_4N_4$	$C_7H_{15}CuIN$
Formula weight	289.53	1158.45	303.64
Temperature	100(2) K	293(2) K	293(2) K
Wavelength	0.71073 Å	0.71073 Å	0.71073 Å
Crystal system	tetragonal	tetragonal	tetragonal
Space group	P -4 21 c	I -4	P 42/n m c
Unit cell dimensions	a = 15.348(4) Å	a = 15.715(3) Å	a = 16.400(3) Å
	b = 15.348(4) Å	b = 15.715(3) Å	b = 16.400(3) Å
	c = 7.4009(17) Å	c = 7.7228(15) Å	c = 7.8196(12) Å
	α = 90°	α = 90°	α = 90°
	β = 90°	β = 90°	β = 90°
	γ = 90°	γ = 90°	γ = 90°
Volume	1743.3(10) $Å^3$	1907.3(8) $Å^3$	2103.3(8) $Å^3$
Z	8	2	8
Density (calculated)	2.206 g/cm^3	2.017 g/cm^3	1.918 g/cm^3

Absorption coefficient	5.971 mm^{-1}	5.456 mm^{-1}	4.952 mm^{-1}
F(000)	1056	1104	1168
Crystal size	0.25 x 0.05 x 0.05 mm^3	0.3 x 0.05 x 0.05 mm^3	0.250 x 0.050 x 0.050 mm^3
θ range for data collection	1.877 to 29.623°	1.833 to 24.687°	1.756 to 26.342°
Reflections collected	8175	5302	5542
Independent reflections	2261 [R_{int} = 0.0650]	1519 [R_{int} = 0.0242]	1151 [R_{int} = 0.0375]
Completeness to θ = 25.242°	99.9%	97.1%	99.3%
Refinement method	Full-matrix least-squares on F^2	Full-matrix least-squares on F^2	Full-matrix least-squares on F^2
Data / restraints / parameters	2261 / 111 / 67	1519 / 0 / 84	1151 / 0 / 53
Goodness-of-fit	1.825	1.009	1.884
Final R indices [I > 2σ(I)]	R_{obs} = 0.0640, wR_{obs} = 0.1371	R_{obs} = 0.0199, wR_{obs} = 0.0434	R_{obs} = 0.0415, wR_{obs} = 0.0524
R indices [all data]	R_{all} = 0.0791, wR_{all} = 0.1413	R_{all} = 0.0230, wR_{all} = 0.0446	R_{all} = 0.0766, wR_{all} = 0.0550
Largest diff. peak and hole	1.521 and -1.407 e·$Å^{-3}$	0.346 and -0.260 e·$Å^{-3}$	0.664 and -0.695 e·$Å^{-3}$

Table S4. Crystallographic and Structural Refinements Details for **10**.

Compounds	Cu_4I_4(quinoline)$_4$ (**10**)
Empirical formula	C_9H_7CuIN
Formula weight	319.60
Temperature	100(2) K
Wavelength	0.71073 Å
Crystal system	monoclinic
Space group	C 2/c
Unit cell dimensions	a = 19.813(12) Å b = 13.776(8) Å c = 16.340(10) Å α = 90° β = 125.477(10)° γ = 90°
Volume	3632(4) $Å^3$
Z	16
Density (calculated)	2.338 g/cm^3
Absorption coefficient	5.743 mm^{-1}
F(000)	2400

Crystal size	0.2 x 0.05 x 0.05 mm^3
θ range for data collection	1.944 to 27.364°
Reflections collected	14720
Independent reflections	4071 [R_{int} = 0.0455]
Completeness to θ = 25.242°	100%
Refinement method	Full-matrix least-squares on F^2
Data / restraints / parameters	4071 / 31 / 192
Goodness-of-fit	1.354
Final R indices [I > 2σ(I)]	R_{obs} = 0.0811, wR_{obs} = 0.1884
R indices [all data]	R_{all} = 0.0901, wR_{all} = 0.1914
Largest diff. peak and hole	4.042 and -4.827 e·$Å^{-3}$

Table S5. Selected bond lengths [Å] and angles [°] for CuI(isoquinoline) (**1**) with estimated standard deviations in parentheses.

Label	Distances (Å)	Label	Angles (°)	Label	Angles (°)
I(1)-Cu(1)	2.6565(19)	Cu(1)-I(1)-Cu(1)#1	64.81(4)	I(1)#1-Cu(1)-I(1)#2	102.84(6)
I(1)-Cu(1)#1	2.6776(12)	Cu(1)-I(1)-Cu(1)#2	64.81(4)	N(1)-Cu(1)-Cu(1)#2	124.11(14)
I(1)-Cu(1)#2	2.6776(12)	Cu(1)#1-I(1)-Cu(1)#2	102.84(6)	I(1)-Cu(1)-Cu(1)#2	57.95(6)
Cu(1)-N(1)	2.064(10)	N(1)-Cu(1)-I(1)	106.6(3)	I(1)#1-Cu(1)-Cu(1)#2	127.13(9)
Cu(1)-I(1)#1	2.6776(12)	N(1)-Cu(1)-I(1)#1	108.37(15)	I(1)#2-Cu(1)-Cu(1)#2	57.24(4)
Cu(1)-I(1)#2	2.6776(12)	I(1)-Cu(1)-I(1)#1	115.19(4)	N(1)-Cu(1)-Cu(1)#1	124.11(14)
Cu(1)-Cu(1)#2	2.859(2)	N(1)-Cu(1)-I(1)#2	108.37(16)	I(1)-Cu(1)-Cu(1)#1	57.95(5)
Cu(1)-Cu(1)#1	2.859(2)	I(1)-Cu(1)-I(1)#2	115.19(4)	I(1)#1-Cu(1)-Cu(1)#1	57.24(4)

Symmetry transformations used to generate equivalent atoms:
(1) -x,-y+1,-z+1 (2) -x,-y,-z+1

Table S6. Selected bond lengths [Å] and angles [°] for CuI(3-methylisoquinoline) (**2**) with estimated standard deviations in parentheses.

Label	Distances (Å)	Label	Angles (°)	Label	Angles (°)
Cu(1)-N(1)	2.033(14)	N(1)-Cu(1)-I(2)	129.2(4)	I(1)-Cu(2)-I(1)#2	105.05(13)
Cu(1)-I(2)	2.636(3)	N(1)-Cu(1)-I(2)#1	102.7(4)	N(2)-Cu(2)-I(2)	102.7(5)
Cu(1)-I(2)#1	2.686(3)	I(2)-Cu(1)-I(2)#1	104.22(13)	I(1)-Cu(2)-I(2)	100.98(12)
Cu(1)-I(1)	2.725(5)	N(1)-Cu(1)-I(1)	104.3(4)	I(1)#2-Cu(2)-I(2)	116.00(14)
Cu(1)-Cu(2)#1	2.865(3)	I(2)-Cu(1)-I(1)	101.21(12)	N(2)-Cu(2)-Cu(1)#2	115.1(5)
Cu(2)-N(2)	2.049(14)	I(2)#1-Cu(1)-I(1)	116.15(14)	I(1)-Cu(2)-Cu(1)#2	114.83(11)
Cu(2)-I(1)	2.623(3)	N(1)-Cu(1)-Cu(2)#1	115.9(4)	I(1)#2-Cu(2)-Cu(1)#2	58.86(11)
Cu(2)-I(1)#2	2.669(3)	I(2)-Cu(1)-Cu(2)#1	114.80(11)	I(2)-Cu(2)-Cu(1)#2	57.15(8)
Cu(2)-I(2)	2.746(5)	I(2)#1-Cu(1)-Cu(2)#1	59.18(11)	Cu(2)-I(1)-Cu(2)#1	105.05(13)
Cu(2)-Cu(1)#2	2.865(3)	I(1)-Cu(1)-Cu(2)#1	56.96(8)	Cu(2)-I(1)-Cu(1)	79.20(12)

I(1)-Cu(2)#1	2.669(3)	N(2)-Cu(2)-I(1)	130.0(5)	Cu(2)#1-I(1)-Cu(1)	64.18(10)
I(2)-Cu(1)#2	2.686(3)	N(2)-Cu(2)-I(1)#2	102.9(5)	Cu(1)-I(2)-Cu(1)#2	104.22(13)

Symmetry transformations used to generate equivalent atoms:
(1) x,y-1,z (2) x,y+1,z

Table S7. Selected bond lengths [Å] and angles [°] for CuI(7-methylquinoline) (**3**) with estimated standard deviations in parentheses.

Label	Distances (Å)	Label	Angles (°)	Label	Angles (°)
I(1)-Cu(1)#1	2.659(6)	Cu(1)#1-I(1)-Cu(1)	62.56(14)	I(1)#1-Cu(1)-I(1)#3	100.33(13)
I(1)-Cu(1)	2.724(6)	Cu(1)#1-I(1)-Cu(1)#2	79.67(13)	I(1)-Cu(1)-I(1)#3	102.91(19)
I(1)-Cu(1)#2	2.725(5)	Cu(1)-I(1)-Cu(1)#2	102.91(19)	N(1)-Cu(1)-Cu(1)#1	136.7(7)
Cu(1)-N(1)	2.03(2)	N(1)-Cu(1)-I(1)#1	123.0(7)	I(1)#1-Cu(1)-Cu(1)#1	59.86(16)
Cu(1)-I(1)#1	2.659(6)	N(1)-Cu(1)-I(1)	102.4(7)	I(1)-Cu(1)-Cu(1)#1	57.58(17)
Cu(1)-I(1)#3	2.725(5)	I(1)#1-Cu(1)-I(1)	117.44(14)	I(1)#3-Cu(1)-Cu(1)#1	112.9(2)
Cu(1)-Cu(1)#1	2.796(8)	N(1)-Cu(1)-I(1)#3	108.9(7)	C(1)-N(1)-Cu(1)	123(2)

Symmetry transformations used to generate equivalent atoms:
(1) -x+1,-y+1,-z+1 (2) x-1,y,z (3) x+1,y,z

Table S8. Selected bond lengths [Å] and angles [°] for CuI(3-methylquinoline) (**4**) with estimated standard deviations in parentheses.

Label	Distances (Å)	Label	Angles (°)	Label	Angles (°)
I(1)-Cu(2)#1	2.655(4)	Cu(2)#1-I(1)-Cu(2)	104.16(15)	I(1)#3-Cu(2)-I(1)#2	99.48(15)
I(1)-Cu(2)	2.659(4)	Cu(2)#1-I(1)-Cu(2)#2	80.52(15)	I(1)-Cu(2)-I(1)#2	117.31(16)
I(1)-Cu(2)#2	2.722(5)	Cu(2)-I(1)-Cu(2)#2	62.69(16)	N(1)-Cu(2)-Cu(2)#2	122.3(10)
Cu(2)-N(1)	2.00(2)	N(1)-Cu(2)-I(1)#3	124.5(10)	I(1)#3-Cu(2)-Cu(2)#2	113.1(2)
Cu(2)-I(1)#3	2.655(4)	N(1)-Cu(2)-I(1)	105.4(8)	I(1)-Cu(2)-Cu(2)#2	59.74(14)
Cu(2)-I(1)#2	2.721(5)	I(1)#3-Cu(2)-I(1)	104.16(15)	I(1)#2-Cu(2)-Cu(2)#2	57.57(16)
Cu(2)-Cu(2)#2	2.800(9)	N(1)-Cu(2)-I(1)#2	106.9(9)	C(1)-N(1)-Cu(2)	136(3)

Symmetry transformations used to generate equivalent atoms:
(1) x-1,y,z (2) -x+2,-y+1,-z+1 (3) x+1,y,z

Table S9. Selected bond lengths [Å] and angles [°] for CuI(4-methylquinoline) (**5**) with estimated standard deviations in parentheses.

Label	Distances (Å)	Label	Angles (°)	Label	Angles (°)
Cu(1)-N(1)	2.030(17)	N(1)-Cu(1)-I(1)	127.4(4)	I(1)-Cu(1)-Cu(1)#3	113.49(17)
Cu(1)-I(1)	2.658(6)	N(1)-Cu(1)-I(1)#1	106.5(4)	I(1)#1-Cu(1)-Cu(1)#3	59.71(16)
Cu(1)-I(1)#1	2.665(6)	I(1)-Cu(1)-I(1)#1	104.5(2)	I(1)#2-Cu(1)-Cu(1)#3	57.06(17)
Cu(1)-I(1)#2	2.742(8)	N(1)-Cu(1)-I(1)#2	102.8(4)	Cu(1)-I(1)-Cu(1)#4	104.5(2)
Cu(1)-Cu(1)#3	2.835(7)	I(1)-Cu(1)-I(1)#2	99.75(11)	Cu(1)-I(1)-Cu(1)#2	80.25(11)

I(1)-Cu(1)#4	2.665(6)	I(1)#1-Cu(1)-I(1)#2	116.77(7)	Cu(1)#4-I(1)-Cu(1)#2	63.23(7)
I(1)-Cu(1)#2	2.742(8)	N(1)-Cu(1)-Cu(1)#3	118.8(5)	C(9)-N(1)-Cu(1)	133.8(14)

Symmetry transformations used to generate equivalent atoms:
(1) x,y+1,z (2) -x+1/2,-y+1/2,-z+1 (3) -x+1/2,-y+3/2,-z+1 (4) x,y-1,z

Table S10. Selected bond lengths [Å] and angles [°] for $Cu_2I_2(Ph_3P)_2$(7-methylquinoline)$_2$ (**6**) with estimated standard deviations in parentheses.

Label	Distances (Å)	Label	Angles (°)	Label	Angles (°)
Cu(1)-N(1)	2.090(3)	N(1)-Cu(1)-P(1)	113.90(8)	I(1)-Cu(1)-I(1)#1	104.15(2)
Cu(1)-P(1)	2.2507(16)	N(1)-Cu(1)-I(1)	113.61(8)	Cu(1)-I(1)-Cu(1)#1	75.85(2)
Cu(1)-I(1)	2.6302(15)	P(1)-Cu(1)-I(1)	116.23(4)	C(9)-N(1)-Cu(1)	118.2(3)
Cu(1)-I(1)#1	2.807(2)	N(1)-Cu(1)-I(1)#1	103.27(8)	C(1)-N(1)-Cu(1)	123.3(2)
I(1)-Cu(1)#1	2.807(2)	P(1)-Cu(1)-I(1)#1	103.63(4)	C(17)-P(1)-Cu(1)	108.26(10)

Symmetry transformations used to generate equivalent atoms:
(1) -x+1,-y+1,-z

Table S11. Selected bond lengths [Å] and angles [°] for Cu_4I_4(2-methylpiperidine)$_4$ (**7**) with estimated standard deviations in parentheses.

Label	Distances (Å)	Label	Angles (°)	Label	Angles (°)
N(1B)-Cu(1)	2.09(2)	Cu(1)#1-I(1)-Cu(1)#2	60.67(6)	N(1)-Cu(1)-I(1)	102.3(6)
I(1)-Cu(1)#1	2.6710(14)	Cu(1)#1-I(1)-Cu(1)	60.48(5)	I(1)#3-Cu(1)-I(1)	113.75(10)
I(1)-Cu(1)#2	2.690(3)	Cu(1)#2-I(1)-Cu(1)	62.86(5)	I(1)#2-Cu(1)-I(1)	108.35(5)
I(1)-Cu(1)	2.706(3)	N(1B)-Cu(1)-I(1)#3	103.9(9)	N(1B)-Cu(1)-Cu(1)#1	147.2(6)
Cu(1)-I(1)#3	2.6710(14)	N(1)-Cu(1)-I(1)#3	105.3(9)	N(1)-Cu(1)-Cu(1)#1	137.9(6)
Cu(1)-I(1)#2	2.690(3)	N(1B)-Cu(1)-I(1)#2	103.2(6)	I(1)#3-Cu(1)-Cu(1)#1	60.02(8)
Cu(1)-Cu(1)#1	2.708(2)	N(1)-Cu(1)-I(1)#2	112.3(7)	I(1)#2-Cu(1)-Cu(1)#1	109.54(8)
Cu(1)-Cu(1)#3	2.708(2)	I(1)#3-Cu(1)-I(1)#2	114.24(9)	I(1)-Cu(1)-Cu(1)#1	59.13(5)
Cu(1)-Cu(1)#2	2.814(3)	N(1B)-Cu(1)-I(1)	113.0(7)	N(1B)-Cu(1)-Cu(1)#3	137.8(6)

Symmetry transformations used to generate equivalent atoms:
(1) y,-x+1,-z (2) -x+1,-y+1,z (3) -y+1,x,-z

Table S12. Selected bond lengths [Å] and angles [°] for Cu_4I_4(4-methylpiperidine)$_4$ (**8**) with estimated standard deviations in parentheses.

Label	Distances (Å)	Label	Angles (°)	Label	Angles (°)
I(1)-Cu(1)	2.6611(10)	Cu(1)-I(1)-Cu(1)#1	61.53(3)	N(1)-Cu(1)-I(1)#1	104.05(13)
I(1)-Cu(1)#1	2.6877(10)	Cu(1)-I(1)-Cu(1)#2	61.43(3)	I(1)-Cu(1)-I(1)#1	110.40(3)
I(1)-Cu(1)#2	2.6956(10)	Cu(1)#1-I(1)-Cu(1)#2	59.31(3)	Cu(1)#3-Cu(1)-I(1)#1	60.20(3)
Cu(1)-N(1)	2.069(5)	N(1)-Cu(1)-I(1)	109.50(15)	I(1)#2-Cu(1)-I(1)#1	116.20(3)
Cu(1)-Cu(1)#3	2.6634(16)	N(1)-Cu(1)-Cu(1)#3	139.49(15)	N(1)-Cu(1)-Cu(1)#1	146.37(13)

Cu(1)-I(1)#2	2.6877(10)	I(1)-Cu(1)-Cu(1)#3	110.996(19)	I(1)-Cu(1)-Cu(1)#1	59.71(4)
Cu(1)-I(1)#1	2.6957(10)	N(1)-Cu(1)-I(1)#2	105.58(13)	Cu(1)#3-Cu(1)-Cu(1)#1	60.875(19)
Cu(1)-Cu(1)#1	2.7360(14)	I(1)-Cu(1)-I(1)#2	110.65(3)	I(1)#2-Cu(1)-Cu(1)#1	108.00(3)
Cu(1)-Cu(1)#2	2.7360(14)	Cu(1)#3-Cu(1)-I(1)#2	60.50(3)	I(1)#1-Cu(1)-Cu(1)#1	58.67(3)
Symmetry transformations used to generate equivalent atoms:					
(1) y+1/2,-x+3/2,-z+1/2 (2) -y+3/2,x-1/2,-z+1/2 (3) -x+2,-y+1,z					

Table S13. Selected bond lengths [Å] and angles [°] for Cu_4I_4(3,5-dimethylpiperidine)$_4$ (**9**) with estimated standard deviations in parentheses.

Label	Distances (Å)	Label	Angles (°)	Label	Angles (°)
I(1)-Cu(1)#1	2.6866(7)	Cu(1)#1-I(1)-Cu(1)	58.23(3)	N(1)-Cu(1)-I(1)	104.63(9)
I(1)-Cu(1)	2.6866(7)	Cu(1)#1-I(1)-Cu(1)#2	59.71(3)	Cu(1)#1-Cu(1)-I(1)	60.885(15)
I(1)-Cu(1)#2	2.6985(11)	Cu(1)-I(1)-Cu(1)#2	59.71(3)	Cu(1)#2-Cu(1)-I(1)	60.37(3)
Cu(1)-N(1)	2.052(6)	N(1)-Cu(1)-Cu(1)#1	142.18(18)	Cu(1)#3-Cu(1)-I(1)	109.35(2)
Cu(1)-Cu(1)#1	2.6143(16)	N(1)-Cu(1)-Cu(1)#2	146.02(9)	N(1)-Cu(1)-I(1)#1	104.63(9)
Cu(1)-Cu(1)#2	2.6808(15)	Cu(1)#1-Cu(1)-Cu(1)#2	60.82(2)	Cu(1)#1-Cu(1)-I(1)#1	60.885(15)
Cu(1)-Cu(1)#3	2.6808(15)	N(1)-Cu(1)-Cu(1)#3	146.02(9)	Cu(1)#2-Cu(1)-I(1)#1	109.35(2)
Cu(1)-I(1)#1	2.6866(7)	Cu(1)#1-Cu(1)-Cu(1)#3	60.82(2)	Cu(1)#3-Cu(1)-I(1)#1	60.37(3)
Cu(1)-I(1)#3	2.6985(11)	Cu(1)#2-Cu(1)-Cu(1)#3	58.37(4)	I(1)-Cu(1)-I(1)#1	115.73(3)
Symmetry transformations used to generate equivalent atoms:					
(1) -x+3/2,-y+1/2,z (2) -y+1,x-1/2,-z+1/2 (3) y+1/2,-x+1,-z+1/2					

Table S14. Selected bond lengths [Å] and angles [°] for Cu_4I_4(quinoline)$_4$ (**10**) with estimated standard deviations in parentheses.

Label	Distances (Å)	Label	Angles (°)	Label	Angles (°)
Cu(2)-N(2)	1.997(15)	N(2)-Cu(2)-I(2)	109.4(5)	C(18B)-N(2B)-Cu(2B)	125(2)
Cu(2)-I(2)	2.535(3)	N(2)-Cu(2)-I(3)	122.1(5)	C(10B)-N(2B)-Cu(2B)	121(2)
Cu(2)-I(3)	2.537(3)	I(2)-Cu(2)-I(3)	124.51(12)	N(1)-Cu(1)-Cu(1)#1	166.5(3)
Cu(2)-Cu(2)#1	2.875(7)	N(2)-Cu(2)-Cu(2)#1	156.9(5)	N(1)-Cu(1)-I(1)	118.5(3)
Cu(2B)-N(2B)	2.000(16)	I(2)-Cu(2)-Cu(2)#1	84.54(10)	Cu(1)#1-Cu(1)-I(1)	61.04(4)
Cu(2B)-Cu(2B)#1	2.158(11)	I(3)-Cu(2)-Cu(2)#1	55.49(8)	N(1)-Cu(1)-I(2)	123.8(3)
Cu(2B)-I(3)	2.657(6)	C(18)-N(2)-Cu(2)	117.7(13)	Cu(1)#1-Cu(1)-I(2)	66.75(7)
Cu(2B)-I(2)#1	2.725(7)	C(10)-N(2)-Cu(2)	122.0(12)	I(1)-Cu(1)-I(2)	105.43(7)
Cu(2B)-I(2)	2.854(6)	N(2B)-Cu(2B)-Cu(2B)#1	173.4(9)	N(1)-Cu(1)-I(2)#1	109.6(3)
Cu(2B)-Cu(1)#1	2.979(6)	N(2B)-Cu(2B)-I(3)	107.4(9)	Cu(1)#1-Cu(1)-I(2)#1	58.83(7)
Cu(1)-N(1)	1.992(11)	Cu(2B)#1-Cu(2B)-I(3)	66.04(12)	I(1)-Cu(1)-I(2)#1	100.09(7)

Cu(1)-Cu(1)#1	2.550(4)	N(2B)-Cu(2B)-I(2)#1	113.0(8)	I(2)-Cu(1)-I(2)#1	94.21(8)
Cu(1)-I(1)	2.633(2)	Cu(2B)#1-Cu(2B)-I(2)#1	70.4(3)	N(1)-Cu(1)-Cu(2B)#1	93.1(3)
Cu(1)-I(2)	2.682(2)	I(3)-Cu(2B)-I(2)#1	113.0(2)	Cu(1)#1-Cu(1)-Cu(2B)#1	86.23(11)
Cu(1)-I(2)#1	2.880(2)	N(2B)-Cu(2B)-I(2)	120.3(8)	I(1)-Cu(1)-Cu(2B)#1	147.27(13)
Cu(1)-Cu(2B)#1	2.979(6)	Cu(2B)#1-Cu(2B)-I(2)	64.1(3)	I(2)-Cu(1)-Cu(2B)#1	57.28(14)
I(1)-Cu(1)#1	2.633(2)	I(3)-Cu(2B)-I(2)	109.0(2)	I(2)#1-Cu(1)-Cu(2B)#1	58.28(13)
I(2)-Cu(2B)#1	2.725(7)	I(2)#1-Cu(2B)-I(2)	93.86(19)	Cu(1)-I(1)-Cu(1)#1	57.91(9)
I(2)-Cu(1)#1	2.880(2)	N(2B)-Cu(2B)-Cu(1)#1	92.8(9)	Cu(2)-I(2)-Cu(1)	106.01(10)
I(3)-Cu(2)#1	2.537(3)	Cu(2B)#1-Cu(2B)-Cu(1)#1	93.76(11)	Cu(1)-I(2)-Cu(2B)#1	66.84(13)
I(3)-Cu(2B)#1	2.657(6)	I(3)-Cu(2B)-Cu(1)#1	159.8(2)	Cu(1)-I(2)-Cu(2B)	86.38(15)

Symmetry transformations used to generate equivalent atoms:
(1) -x+1,y,-z+1/2

Table S15. Anisotropic displacement parameters ($Å^2x10^3$) for CuI(isoquinoline) **1** at 100(2) K with estimated standard deviations in parentheses.

Label	U_{11}	U_{22}	U_{33}	U_{12}	U_{13}	U_{23}
I(1)	46(1)	29(1)	37(1)	0	18(1)	0
Cu(1)	40(1)	47(1)	46(1)	0	14(1)	0
N(1)	36(5)	45(6)	36(5)	0	13(4)	0
C(7)	42(7)	63(9)	44(7)	0	21(6)	0
C(6)	42(8)	124(18)	70(10)	0	30(7)	0
C(2)	32(7)	41(9)	37(7)	9(7)	18(6)	7(7)
C(1)	36(8)	48(9)	35(7)	1(7)	13(6)	-7(7)
C(9)	46(9)	55(10)	44(8)	1(8)	18(7)	-9(8)
C(8)	56(10)	53(10)	44(8)	8(8)	30(8)	-5(8)
C(3)	46(9)	48(10)	54(10)	-3(9)	10(8)	0(9)
C(4)	54(11)	63(12)	53(10)	-2(10)	19(9)	5(10)
C(5)	36(9)	59(14)	82(14)	-3(9)	5(9)	17(12)

The anisotropic displacement factor exponent takes the form: $-2\pi^2[h^2a^{*2}U_{11} + \ldots + 2hka^*b^*U_{12}]$.

Table S16. Anisotropic displacement parameters ($Å^2x10^3$) for CuI(3-methylisoquinoline) **2** at 299(2) K with estimated standard deviations in parentheses.

Label	U_{11}	U_{22}	U_{33}	U_{12}	U_{13}	U_{23}
C(1)	48(11)	42(12)	47(11)	1(9)	-4(9)	-2(10)
C(2)	55(13)	54(14)	51(12)	-5(10)	-16(10)	4(11)
C(3)	34(11)	62(13)	34(12)	-6(10)	-8(8)	0(10)

C(4)	55(16)	68(16)	70(20)	14(11)	-21(14)	-4(12)
C(5)	25(10)	60(14)	120(20)	3(9)	-12(12)	3(14)
C(6)	36(12)	51(15)	110(20)	7(10)	16(13)	-1(15)
C(7)	78(16)	43(14)	63(16)	7(12)	-24(13)	-4(13)
C(8)	30(11)	31(10)	59(18)	6(8)	-13(11)	-11(10)
C(9)	33(10)	77(17)	42(11)	7(10)	-7(8)	-17(11)
C(10)	100(20)	60(15)	11(10)	24(12)	0(11)	1(8)
C(11)	43(11)	49(12)	36(10)	-10(9)	5(8)	1(9)
C(12)	41(11)	78(15)	35(9)	-3(10)	-9(8)	-5(12)
C(13)	31(11)	48(12)	73(18)	0(9)	5(10)	20(13)
C(14)	19(10)	65(14)	54(15)	-3(8)	-15(10)	18(10)
C(15)	44(11)	43(12)	97(19)	-2(9)	-5(11)	14(13)
C(16)	59(15)	59(15)	80(16)	9(12)	12(12)	-7(14)
C(17)	38(12)	98(19)	60(15)	2(13)	11(10)	-24(15)
C(18)	34(11)	41(11)	42(15)	-7(8)	2(10)	4(9)
C(19)	44(11)	33(10)	48(11)	5(8)	-1(9)	-15(9)
C(20)	35(12)	100(20)	60(20)	8(10)	-9(12)	-25(12)
Cu(1)	34(2)	51(2)	49(2)	7(1)	0(2)	-3(2)
Cu(2)	39(2)	49(2)	58(2)	2(2)	-1(2)	-2(2)
I(1)	44(1)	34(1)	38(1)	3(1)	10(1)	0(1)
I(2)	41(1)	34(1)	33(1)	6(1)	8(1)	2(2)
N(1)	44(8)	44(9)	32(8)	-8(6)	-2(6)	-8(7)
N(2)	40(8)	46(10)	49(10)	1(7)	-3(7)	-6(8)

The anisotropic displacement factor exponent takes the form: $-2\pi^2[h^2a^{*2}U_{11} + \ldots + 2hka^*b^*U_{12}]$.

Table S17. Anisotropic displacement parameters ($Å^2x10^3$) for CuI(7-methylquinoline) **3** at 289(2) K with estimated standard deviations in parentheses.

Label	U_{11}	U_{22}	U_{33}	U_{12}	U_{13}	U_{23}
I(1)	19(1)	41(1)	49(2)	-4(1)	12(1)	-12(1)
Cu(1)	41(2)	41(2)	55(2)	1(2)	15(2)	4(2)
N(1)	41(14)	33(12)	57(16)	0(10)	13(12)	5(10)
C(10)	46(19)	110(30)	25(15)	-2(18)	8(14)	7(17)
C(1)	90(30)	17(13)	100(30)	16(14)	20(20)	-13(15)
C(2)	90(30)	17(14)	100(30)	3(15)	-10(20)	0(15)
C(9)	21(14)	70(20)	70(20)	-13(13)	9(15)	21(17)
C(4)	26(16)	70(20)	80(30)	-24(14)	-11(16)	28(18)
C(7)	32(16)	110(30)	45(18)	-16(17)	-5(14)	36(19)
C(3)	52(15)	90(20)	72(18)	22(14)	-17(14)	51(15)

C(6)	60(30)	130(40)	50(20)	-40(30)	-10(20)	0(20)
C(8)	52(15)	90(20)	72(18)	22(14)	-17(14)	51(15)
C(5)	80(30)	150(50)	80(30)	-30(30)	30(30)	50(30)

The anisotropic displacement factor exponent takes the form: $-2\pi^2[h^2a^{*2}U_{11} + \ldots + 2hka^*b^*U_{12}]$.

Table S18. Anisotropic displacement parameters ($Å^2x10^3$) for CuI(3-methylquinoline) **4** at 289(2) K with estimated standard deviations in parentheses.

Label	U_{11}	U_{22}	U_{33}	U_{12}	U_{13}	U_{23}
I(1)	34(1)	45(2)	46(1)	-3(2)	-2(1)	6(2)
Cu(2)	51(2)	50(2)	53(2)	-1(2)	-6(2)	-11(2)
N(1)	76(19)	38(16)	90(20)	-34(15)	23(17)	-38(15)
C(2)	80(9)	80(10)	82(10)	-24(9)	11(7)	-32(9)
C(9)	80(9)	80(10)	82(10)	-24(9)	11(7)	-32(9)
C(7)	80(9)	80(10)	82(10)	-24(9)	11(7)	-32(9)
C(8)	80(9)	80(10)	82(10)	-24(9)	11(7)	-32(9)
C(10)	50(20)	190(50)	120(40)	50(30)	20(20)	110(40)
C(4)	80(9)	80(10)	82(10)	-24(9)	11(7)	-32(9)
C(6)	80(9)	80(10)	82(10)	-24(9)	11(7)	-32(9)
C(1)	80(9)	80(10)	82(10)	-24(9)	11(7)	-32(9)
C(3)	80(9)	80(10)	82(10)	-24(9)	11(7)	-32(9)
C(5)	80(9)	80(10)	82(10)	-24(9)	11(7)	-32(9)

The anisotropic displacement factor exponent takes the form: $-2\pi^2[h^2a^{*2}U_{11} + \ldots + 2hka^*b^*U_{12}]$.

Table S19. Anisotropic displacement parameters ($Å^2x10^3$) for CuI(4-methylquinoline) **5** at 289(2) K with estimated standard deviations in parentheses.

Label	U_{11}	U_{22}	U_{33}	U_{12}	U_{13}	U_{23}
C(1)	78(8)	48(8)	31(7)	3(6)	-11(7)	7(6)
C(2)	77(8)	52(8)	80(11)	-7(7)	-17(8)	-6(9)
C(3)	80(6)	65(7)	69(7)	-21(5)	6(6)	-21(6)
C(4)	35(6)	73(9)	45(8)	-11(6)	9(6)	-27(8)
C(5)	80(6)	65(7)	69(7)	-21(5)	6(6)	-21(6)
C(6)	77(8)	52(8)	80(11)	-7(7)	-17(8)	-6(9)
C(7)	78(8)	48(8)	31(7)	3(6)	-11(7)	7(6)
C(8)	80(6)	65(7)	69(7)	-21(5)	6(6)	-21(6)
C(9)	35(6)	73(9)	45(8)	-11(6)	9(6)	-27(8)
C(10)	180(20)	110(20)	100(20)	-24(19)	2(18)	0(20)
Cu(1)	56(2)	50(2)	40(2)	4(1)	13(1)	3(2)
I(1)	41(1)	32(1)	38(1)	2(1)	0(1)	-1(1)
N(1)	80(6)	65(7)	69(7)	-21(5)	6(6)	-21(6)

The anisotropic displacement factor exponent takes the form: $-2\pi^2[h^2a^{*2}U_{11} + \ldots + 2hka^*b^*U_{12}]$.

Table S20. Anisotropic displacement parameters ($Å^2x10^3$) for $Cu_2I_2(Ph_3P)_2$(7-methylquinoline)$_2$ **6** at 298(2) K with estimated standard deviations in parentheses.

Label	U_{11}	U_{22}	U_{33}	U_{12}	U_{13}	U_{23}
C(1)	40(2)	34(2)	66(2)	0(2)	-3(2)	-11(2)
C(2)	53(2)	59(2)	71(3)	-1(2)	-6(2)	-27(2)
C(3)	78(3)	85(3)	79(3)	-10(2)	-15(2)	-38(3)
C(4)	108(4)	114(4)	95(4)	7(3)	2(3)	-67(4)
C(5)	89(4)	105(4)	105(4)	34(3)	2(3)	-53(3)
C(6)	56(2)	56(2)	83(3)	11(2)	1(2)	-19(2)
C(7)	54(2)	80(3)	94(4)	30(2)	0(2)	-9(3)
C(8)	49(2)	71(3)	79(3)	16(2)	-14(2)	3(2)
C(9)	49(2)	50(2)	57(2)	7(2)	-13(2)	-3(2)
C(10)	110(4)	162(6)	104(4)	-14(4)	-33(4)	-68(4)
C(11)	43(2)	35(2)	38(2)	5(2)	-12(2)	-11(2)
C(12)	61(2)	53(2)	56(2)	-9(2)	-23(2)	-9(2)
C(13)	78(3)	77(3)	62(3)	-3(2)	-39(2)	-19(2)
C(14)	79(3)	69(2)	41(2)	7(2)	-24(2)	-11(2)
C(15)	62(2)	70(2)	37(2)	-5(2)	-9(2)	-4(2)
C(16)	49(2)	57(2)	41(2)	-5(2)	-11(2)	-9(2)
C(17)	43(2)	39(2)	31(2)	-4(2)	-11(2)	0(2)
C(18)	45(2)	43(2)	57(2)	-2(2)	-14(2)	-2(2)
C(19)	42(2)	68(2)	67(3)	-1(2)	-16(2)	6(2)
C(20)	53(2)	100(3)	49(2)	-20(2)	-26(2)	10(2)
C(21)	76(3)	95(3)	45(2)	-30(2)	-22(2)	-15(2)
C(22)	61(2)	65(2)	40(2)	-11(2)	-12(2)	-16(2)
C(23)	41(2)	34(2)	36(2)	5(2)	-14(2)	-10(2)
C(24)	41(2)	38(2)	41(2)	1(2)	-13(2)	-11(2)
C(25)	43(2)	52(2)	56(2)	6(2)	-13(2)	-25(2)
C(26)	57(2)	53(2)	63(2)	20(2)	-28(2)	-31(2)
C(27)	84(3)	36(2)	60(2)	13(2)	-26(2)	-13(2)
C(28)	69(2)	38(2)	43(2)	3(2)	-10(2)	-7(2)
Cu(1)	41(1)	34(1)	53(1)	3(1)	-11(1)	-7(1)
I(1)	40(1)	46(1)	47(1)	-1(1)	-15(1)	-10(1)
N(1)	40(2)	35(2)	57(2)	3(2)	-5(2)	-6(2)
P(1)	36(1)	31(1)	34(1)	1(1)	-8(1)	-7(1)

The anisotropic displacement factor exponent takes the form: $-2\pi^2[h^2a^{*2}U_{11} + \ldots + 2hka^*b^*U_{12}]$.

Table S21. Anisotropic displacement parameters ($Å^2x10^3$) for Cu_4I_4(2-methylpiperidine)$_4$ **7** at 100(2) K with estimated standard deviations in parentheses.

Label	U_{11}	U_{22}	U_{33}	U_{12}	U_{13}	U_{23}
I(1)	48(1)	43(1)	18(1)	-3(1)	5(1)	9(1)
Cu(1)	39(1)	49(1)	17(1)	7(2)	-4(1)	5(2)

The anisotropic displacement factor exponent takes the form: $-2\pi^2[h^2a^{*2}U_{11} + \ldots + 2hka^*b^*U_{12}]$.

Table S22. Anisotropic displacement parameters ($Å^2x10^3$) for Cu_4I_4(4-methylpiperidine)$_4$ **8** at 293(2) K with estimated standard deviations in parentheses.

Label	U_{11}	U_{22}	U_{33}	U_{12}	U_{13}	U_{23}
I(1)	57(1)	73(1)	48(1)	3(1)	-14(1)	-12(1)
Cu(1)	63(1)	71(1)	48(1)	-8(1)	7(1)	1(1)
N(1)	62(3)	55(2)	43(3)	-7(2)	-2(3)	2(3)
C(6)	92(6)	135(7)	90(8)	-45(6)	22(5)	11(6)
C(1)	93(5)	69(4)	68(6)	-26(3)	14(5)	-12(4)
C(3)	71(5)	117(6)	54(5)	-43(5)	-8(4)	10(4)
C(5)	58(3)	84(4)	82(6)	6(3)	5(4)	36(4)
C(4)	53(3)	87(5)	76(6)	5(3)	3(3)	21(4)
C(2)	101(6)	70(4)	67(6)	-41(4)	2(4)	-3(4)

The anisotropic displacement factor exponent takes the form: $-2\pi^2[h^2a^{*2}U_{11} + \ldots + 2hka^*b^*U_{12}]$.

Table S23. Anisotropic displacement parameters ($Å^2x10^3$) for Cu_4I_4(3,5-dimethylpiperidine)$_4$ **9** at 293(2) K with estimated standard deviations in parentheses.

Label	U_{11}	U_{22}	U_{33}	U_{12}	U_{13}	U_{23}
I(1)	71(1)	111(1)	67(1)	0	15(1)	0
Cu(1)	89(1)	72(1)	70(1)	0	0	-12(1)
N(1)	140(6)	77(4)	77(5)	0	0	-9(4)
C(4)	195(7)	105(5)	108(6)	-68(5)	20(5)	-26(4)
C(3)	700(60)	73(10)	106(13)	0	0	-21(10)
C(2)	402(14)	126(7)	85(7)	-136(9)	33(9)	-44(7)
C(1)	493(18)	283(12)	138(10)	-288(13)	70(10)	-68(8)

The anisotropic displacement factor exponent takes the form: $-2\pi^2[h^2a^{*2}U_{11} + \ldots + 2hka^*b^*U_{12}]$.

Table S24. Anisotropic displacement parameters ($Å^2x10^3$) for CuI(quinoline) **10** at 100(2) K with estimated standard deviations in parentheses.

Label	U_{11}	U_{22}	U_{33}	U_{12}	U_{13}	U_{23}
Cu(2)	20(2)	30(2)	40(2)	1(1)	15(2)	-8(2)
N(2)	16(4)	12(4)	19(4)	-4(3)	7(4)	-7(4)
C(10)	15(5)	10(4)	23(6)	-4(4)	10(5)	-6(4)

C(11)	24(6)	19(6)	29(6)	-2(5)	16(5)	-5(5)
C(12)	21(5)	18(5)	23(6)	-3(4)	9(5)	-1(5)
C(13)	16(5)	17(5)	23(6)	4(4)	3(4)	-4(4)
C(14)	16(5)	21(5)	27(6)	1(4)	13(5)	-4(5)
C(15)	17(5)	9(4)	25(5)	0(4)	9(4)	2(4)
C(16)	23(6)	14(5)	32(6)	7(5)	17(5)	7(5)
C(17)	26(6)	18(5)	22(5)	5(5)	11(5)	7(4)
C(18)	26(6)	15(5)	19(5)	1(4)	8(5)	-6(5)
Cu(2B)	20(2)	30(2)	40(2)	1(1)	15(2)	-8(2)
C(18B)	26(6)	15(5)	19(5)	1(4)	8(5)	-6(5)
C(17B)	26(6)	18(5)	22(5)	5(5)	11(5)	7(4)
C(16B)	23(6)	14(5)	32(6)	7(5)	17(5)	7(5)
C(11B)	24(6)	19(6)	29(6)	-2(5)	16(5)	-5(5)
C(14B)	16(5)	21(5)	27(6)	1(4)	13(5)	-4(5)
C(15B)	17(5)	9(4)	25(5)	0(4)	9(4)	2(4)
N(2B)	16(4)	12(4)	19(4)	-4(3)	7(4)	-7(4)
C(12B)	21(5)	18(5)	23(6)	-3(4)	9(5)	-1(5)
C(10B)	15(5)	10(4)	23(6)	-4(4)	10(5)	-6(4)
C(13B)	16(5)	17(5)	23(6)	4(4)	3(4)	-4(4)
C(1)	15(5)	10(4)	23(6)	-4(4)	10(5)	-6(4)
C(2)	24(6)	19(6)	29(6)	-2(5)	16(5)	-5(5)
C(3)	21(5)	18(5)	23(6)	-3(4)	9(5)	-1(5)
C(4)	16(5)	17(5)	23(6)	4(4)	3(4)	-4(4)
C(5)	16(5)	21(5)	27(6)	1(4)	13(5)	-4(5)
C(6)	17(5)	9(4)	25(5)	0(4)	9(4)	2(4)
C(7)	23(6)	14(5)	32(6)	7(5)	17(5)	7(5)
C(8)	26(6)	18(5)	22(5)	5(5)	11(5)	7(4)
C(9)	26(6)	15(5)	19(5)	1(4)	8(5)	-6(5)
Cu(1)	14(1)	26(1)	27(1)	3(1)	11(1)	4(1)
I(1)	20(1)	17(1)	62(1)	0	23(1)	0
I(2)	16(1)	26(1)	21(1)	-4(1)	8(1)	1(1)
I(3)	22(1)	19(1)	26(1)	0	15(1)	0
N(1)	16(4)	12(4)	19(4)	-4(3)	7(4)	-7(4)

The anisotropic displacement factor exponent takes the form: $-2\pi^2[h^2a^{*2}U_{11} + \ldots + 2hka^*b^*U_{12}]$.

Section S2. Calculated and experimental PXRD.

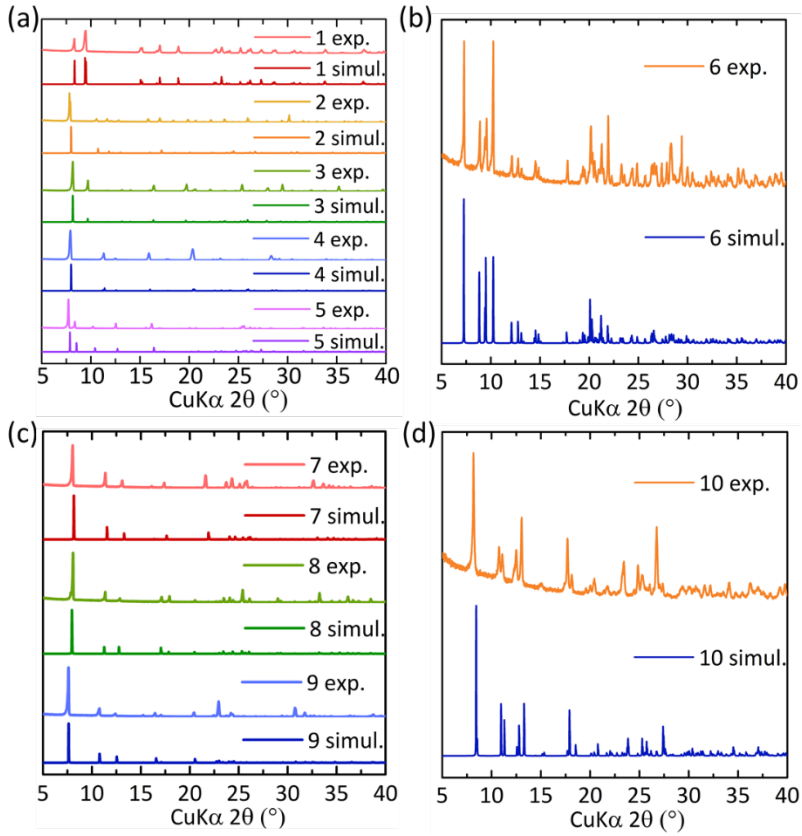

Figure S1. Simulated and experimental PXRD patterns of **1**-**10**. All the compounds are pure phases.

Section S3. Structure plots.

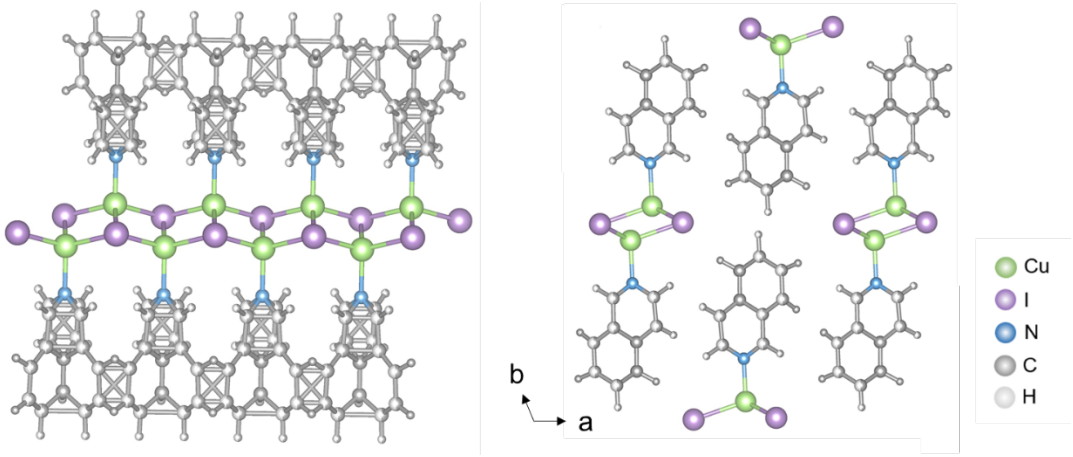

Figure S2. Crystal structure of CuI(isoquinoline) (**1**). Organic ligand isoquinoline has disorder in two directions along CuI chains.

Section S4. Calculated band gap of selected compounds.

Table S25. Calculated and estimated band gap of selected compounds.

Compounds	Calculated Bandgap	Estimated Bandgap (eV)

	(eV)	
CuI(7-methylquinoline) (**3**)	1.00	2.56
$Cu_2I_2(Ph_3P)_2$(7-methylquinoline)$_2$ (**6**)	1.34	2.56
Cu_4I_4(4-methylpiperidine)$_4$ (**8**)	2.54	2.57
Cu_4I_4(quinoline)$_4$ (**10**)	1.18	2.73

Section S5. Additional PL data.

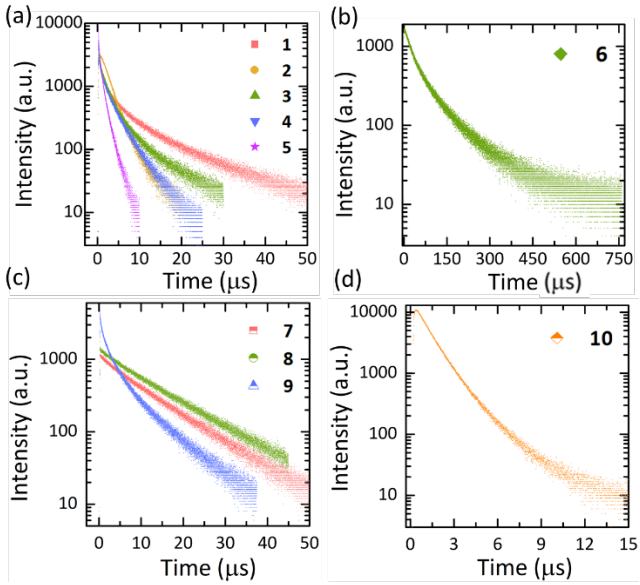

Figure S3. PL decay spectra of **1-10** at room temperature.

Table S26. Lifetime fitting parameters for **1-10** at room temperature.

Compounds	A_1	τ_1 (μs)	A_2	τ_2 (μs)	A_3	τ_3 (μs)	τ_{av}	R^2
1	1232.66	0.61	964.96	2.58	501.76	11.79	3.39	0.9979
2 (HE)	3131.58	2.30					2.30	0.9980
2 (LE)	3360.26	2.07	220.49	61.18			5.71	0.9986
3	1271.59	0.18	1921.25	1.55	667.81	5.67	1.81	0.9989
4	1857.13	0.09	1323.96	0.70	1425.57	3.40	1.29	0.9986
5	2434.89	0.04	3565.87	0.28	2557.13	1.21	0.49	0.9995
6	1024.22	25.77	595.75	102.28			53.90	0.9978
7	188.70	2.88	934.25	11.44			10.00	0.9964
8	198.03	2.98	1161.42	12.73			11.31	0.9968
9	1220.32	0.19	1879.50	1.46	1158.26	6.41	2.44	0.9988
10	10032.15	0.92	2400.89	1.91			1.11	0.9997

Table S27. Nearest centroid-to-centroid distance d_{cc} of inorganic motif in **1-10.**

Compounds	**1**	**2**	**3**	**4**	**5**
d_{cc} (Å)	10.422	10.804	11.253	10.722	10.473
Compounds	**6**	**7**	**8**	**9**	**10**

d_{cc} (Å)	9.764	7.401	7.723	7.82	8.348

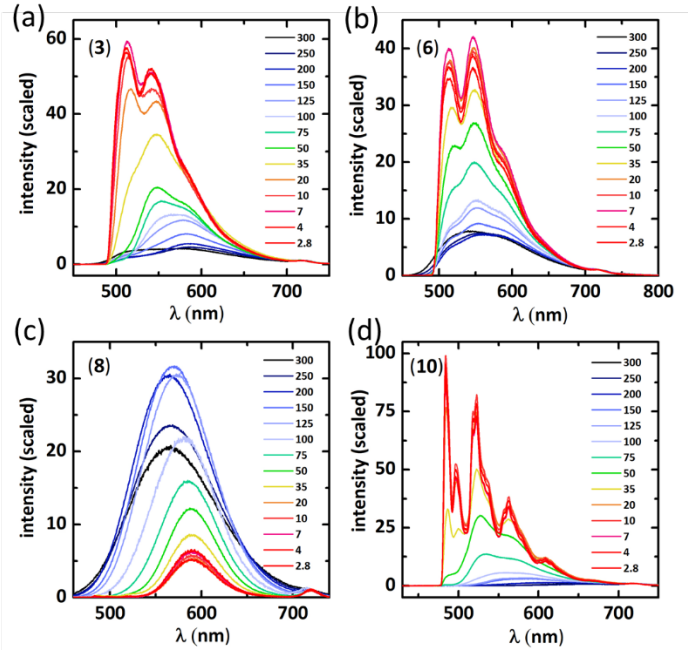

Figure S4. Temperature-dependent photoluminescence (PL) spectra normalized at Rayleigh scattering peak 720 nm of (a) CuI chain structure **3**, (b) Cu_2I_2 rhomboid dimer structure **6**, (c) Cu_4I_4 cubane tetramer structure **8**, and (d) Cu_4I_4 octahedral tetramer structure **10** recorded between 2.8 K and 300 K under 360 nm excitation, to show the absolute PL intensity change.

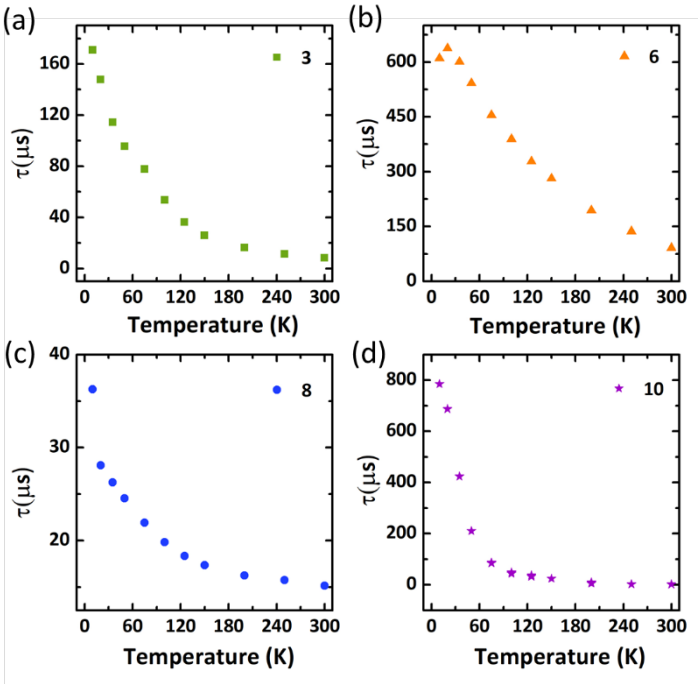

Figure S5. Temperature-dependent lifetimes of (a) CuI chain structure **3**, (b) Cu_2I_2 rhomboid dimer structure **6**, (c) Cu_4I_4 cubane tetramer structure **8**, and (d) Cu_4I_4 octahedral tetramer structure **10** recorded between 10 K and 300 K under 360 nm excitation.

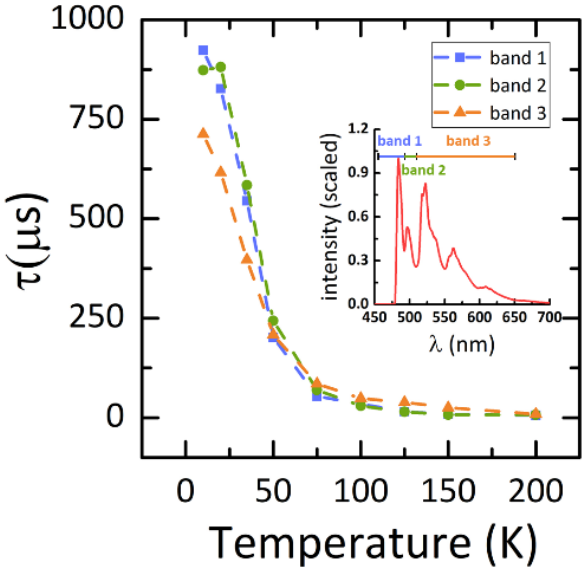

Figure S6. Temperature-dependent lifetimes of different emission bands for compound **10** recorded between 10 K and 200 K.

Section S6. Additional DFT calculation results

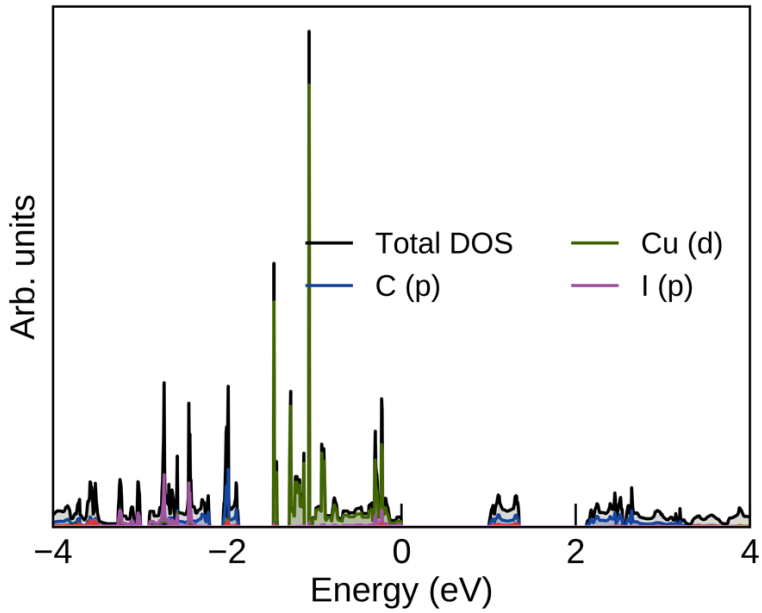

Figure S7. DFT-calculated density of states for CuI(7-methylquinoline) (**3**).

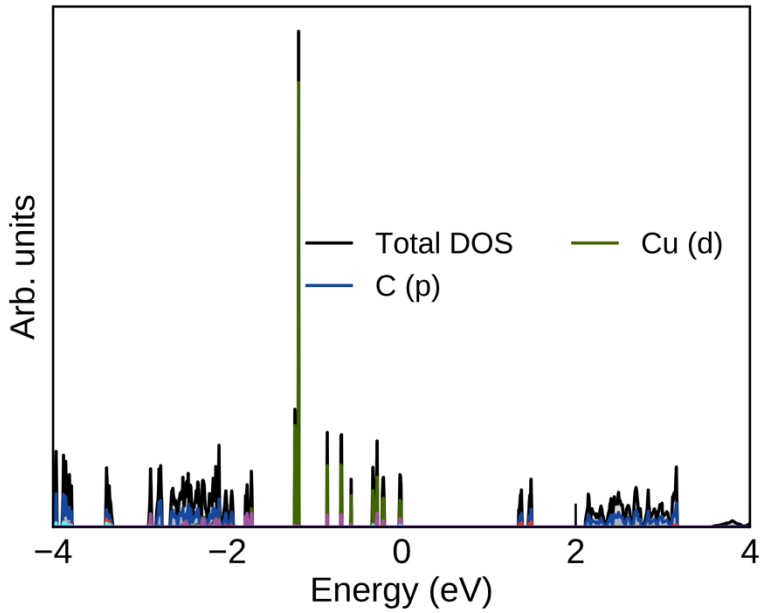

Figure S8. DFT-calculated density of states for Cu_2I_2(triphenylphosphine)$_2$(7-methylquinoline)$_2$ **(6)**.

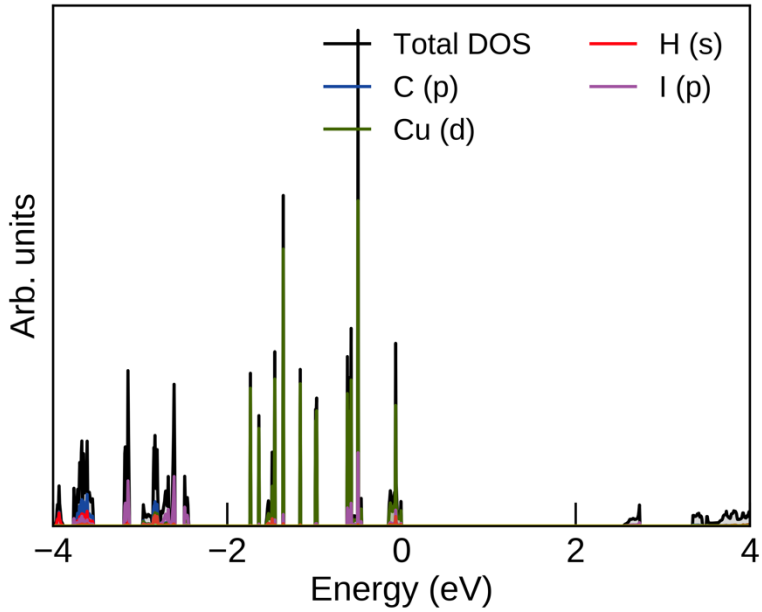

Figure S9. DFT-calculated density of states for Cu_4I_4(4-methylpiperidine)$_4$ **(8)**.

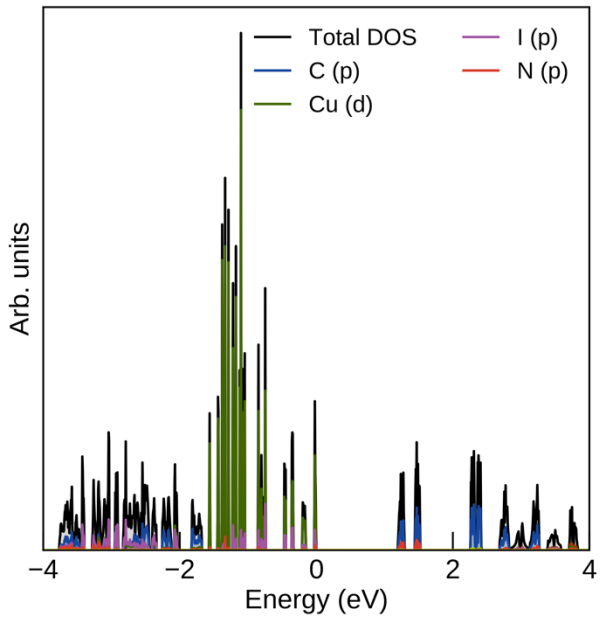

Figure S10. DFT-calculated density of states for Cu_4I_4(quinoline)$_4$ **(10)**.